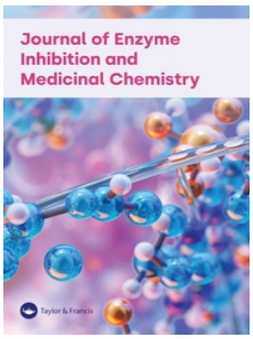

Journal of Enzyme Inhibition and Medicinal Chemistry

ISSN: 1475-6366 (Print) 1475-6374 (Online) Journal homepage: www.tandfonline.com/journals/ienz20

# Design, synthesis, anticancer activity, and mechanistic investigation of 4,5,6,7-tetrahydrobenzo[*b*]thiophene carboxamides as CDK-2 inhibitors: *in vitro* and *in silico* DFT and molecular docking study

**Kurls E. Anwer, Ramadan M. Ramadan, Eman S. Nossier , Najla A. Altwaijry , Asmaa Saleh , Stefan Bräse & Ebtehal M. Husseiny**

**To cite this article:** Kurls E. Anwer, Ramadan M. Ramadan, Eman S. Nossier , Najla A. Altwaijry , Asmaa Saleh , Stefan Bräse & Ebtehal M. Husseiny (2026) Design, synthesis, anticancer activity, and mechanistic investigation of 4,5,6,7-tetrahydrobenzo[*b*]thiophene carboxamides as CDK-2 inhibitors: *in vitro* and *in silico* DFT and molecular docking study, Journal of Enzyme Inhibition and Medicinal Chemistry, 41:1, 2656826, DOI: 10.1080/14756366.2026.2656826

**To link to this article:** https://doi.org/10.1080/14756366.2026.2656826

JOURNAL OF ENZYME INHIBITION AND MEDICINAL CHEMISTRY
2026, VOL. 41, NO. 1, 2656826
https://doi.org/10.1080/14756366.2026.2656826

Taylor & Francis
by informa

RESEARCH ARTICLE

OPEN ACCESS Check for updates

# Design, synthesis, anticancer activity, and mechanistic investigation of 4,5,6,7-tetrahydrobenzo[*b*]thiophene carboxamides as CDK-2 inhibitors: *in vitro* and *in silico* DFT and molecular docking study

Kurls E. Anwer[a], Ramadan M. Ramadan[a], Eman S. Nossier[b], Najla A. Altwaijry[c], Asmaa Saleh[c], Stefan Bräse[d] and Ebtehal M. Husseiny[e]

[a]Chemistry Department, Faculty of Science, Ain Shams University, Cairo, Egypt; [b]Pharmaceutical Medicinal Chemistry and Drug Design Department, Faculty of Pharmacy (Girls), Al-Azhar University, Cairo, Egypt; [c]Department of Pharmaceutical Sciences, College of Pharmacy, Princess Nourah bint Abdulrahman University, Riyadh, Saudi Arabia; [d]Institute of Biological and Chemical Systems, IBCS-FMS, Karlsruhe Institute of Technology, Karlsruhe, Germany; [e]Pharmaceutical Organic Chemistry Department, Faculty of Pharmacy (Girls), Al-Azhar University, Cairo, Egypt

**ABSTRACT**

Utilising drug design methodologies including bioisosteric modification and substituents variation, sets of 4,5,6,7-tetrahydrobenzo[*b*]thiophene carboxamides were synthesised, by conventional heating and eco-friendly microwave-assisted techniques, as CDK-2 inhibitors. These entities were assessed for their antitumor effects against hepatic HepG-2 and breast MCF-7 and MDA-MB-231 carcinomas, in which dimethoxy **5** and dimethyl-bearing analogues **6** and **11** demonstrated significant cytotoxicity and selectivity against the examined cancer cells. Consequently, they were chosen for further assays to determine their mechanism. The findings suggest that these compounds may exert cytotoxicity by inhibiting CDK-2. Compound **11** displayed the highest CDK-2 inhibition, exceeding roscovitine by nearly threefold. Besides, it arrested the MDA-MB-231 cell cycle at the G0/G1 phase by apoptotic stimulation. Molecular modelling showed strong binding of the bioactive analogues to the active pocket of CDK-2 receptor, suggesting their potential as lead inhibitors.

**GRAPHICAL ABSTRACT**

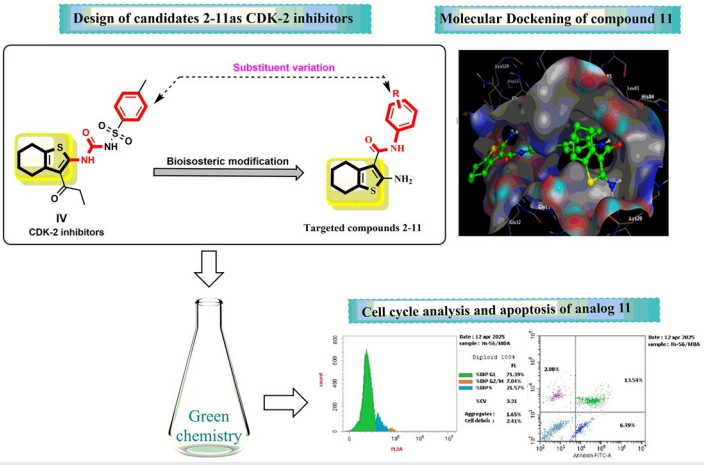


**ARTICLE HISTORY**
Received 20 January 2026
Revised 2 March 2026
Accepted 2 April 2026

**KEYWORDS**
Anticancer; CDK-2; DFT; synthesis; tetrahydrobenzo[*b*] thiophene

**CONTACT** Ebtehal M. Husseiny ebtehal.ouf@azhar.edu.eg Pharmaceutical Organic Chemistry Department, Faculty of Pharmacy (Girls), Al-Azhar University, Nasr City, Cairo11754, Egypt; Stefan Bräse braese@kit.edu Institute of Biological and Chemical Systems, IBCS-FMS, Karlsruhe Institute of Technology, 76131 Karlsruhe, Germany

Supplemental data for this article can be accessed online at https://doi.org/10.1080/14756366.2026.2656826.

## Introduction

Cancer is the primary cause of mortality globally[1]. Despite substantial advancements in cancer therapy, certain restrictions persist. These drawbacks include side effects, non-selectivity for cancer cells, and the emergence of numerous drug-resistant carcinomas[2]. Therefore, considerable effort is being made to inhibit tumour growth by employing newly prepared compounds[3]. To design and develop safer, more selective anticancer medications, it is critical to understand the mechanisms that control the cell cycle[4].

Cyclin-dependent kinases (CDKs) are enzymes that are responsible for transferring a phosphate moiety from adenosine triphosphate to proteins with serine/threonine residues[5]. Human cells contain many types of CDKs, which are divided into transcription-associated and cell-cycle-associated categories[6]. CDKs bind to cyclins and play a critical role in regulating cell cycle progression, transcription, and apoptosis[7]. Hence, CDKs are considered important targets in cancer therapy due to their roles in cell cycle regulation and transcription, as well as their overexpression in numerous cancer types[8,9]. The overexpression of CDK-2 was noted in various tumours, including breast[10], liver[11], kidney[12], ovary[13], prostate[14], and colon cancers[15]. Consequently, CDK-2 has attracted close attention recently as a crucial target in drug discovery[16].

Carboxamide-containing heterocycles have several biological applications in pharmaceutical chemistry, including anticancer[17], anti-inflammatory[18], antimicrobial[19], antiviral[20], analgesic[21], and antimalarial[22] effects. A literature survey showed that carboxamide-containing heterocycles play a crucial role as anti-tumor agents[8]. Milciclib is a promising selective ATP-competitive CDK-2 inhibitor ($IC_{50}$ = 45 nM) that entered phase 2 clinical trials for the treatment of hepatocellular carcinoma. AT7519 is a pan-multi-CDK inhibitor 1, 2, 4, 6, and 9 ($IC_{50}$ range = 10–210 nM) that entered phase 2 clinical trials for the management of chronic lymphocytic leukaemia. Also, SNS-032 is a CDK-2 inhibitor ($IC_{50}$ = 48 nM) used in the treatment of chronic lymphocytic leukaemia, but it is currently in a phase 1 clinical trial. PHA-793887 is a potent, selective CDK-2 inhibitor ($IC_{50}$ = 8 nM) in phase 1 clinical trials for the treatment of metastatic solid tumours[8]. It was reported that pyrimidine carboxamide analogue **I** exhibited promising antitumor activity against MDA-MB-468 through CDK-2 inhibition, apoptosis induction, and cell cycle arrest. The importance of the carboxamide moiety in compound **I** was confirmed by its molecular docking, which illustrated a hydrogen bond (HB) formation with Gln131 residue (Figure 1)[17].

Thiophenes and their fused hybrids have attracted the attention of numerous chemists owing to their fascinating biological activities, including antitumor[23,24], antimicrobial[25], anti-influenza[26],

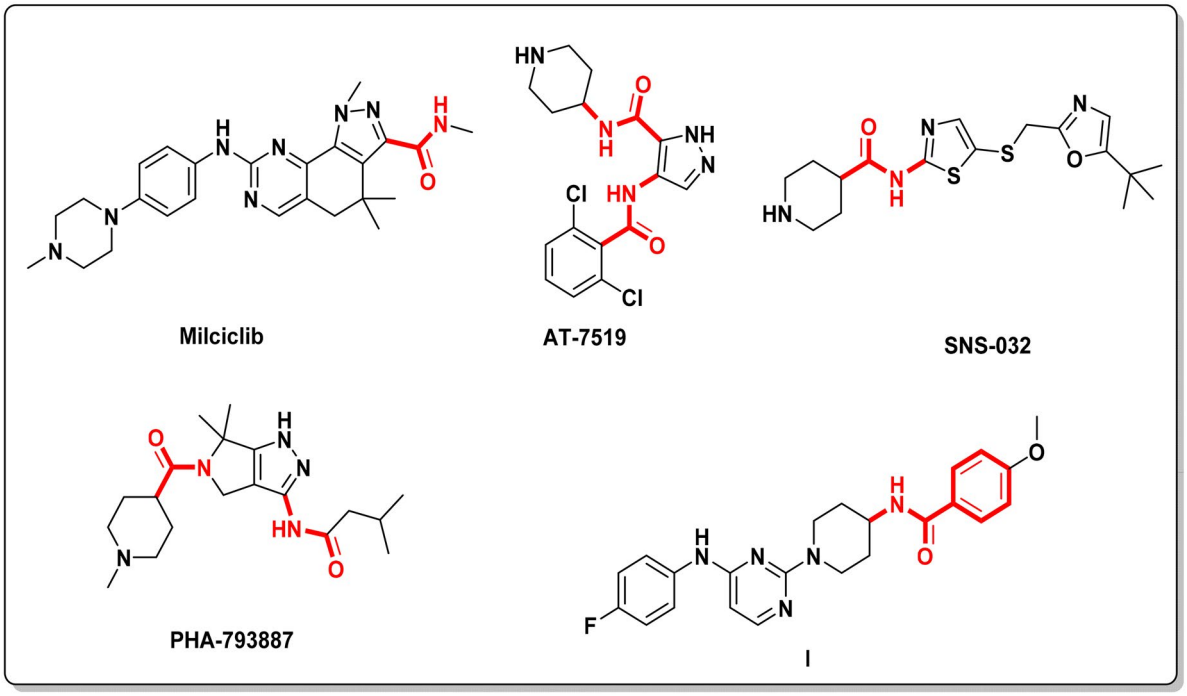


**Figure 1.** Carboxamide-containing compounds as potent CDK-2 inhibitors.

anti-inflammatory[27], and antioxidant[23] effects. Tetrahydrobenzo[*b*]thienothiazoloandrostane **II** exhibited promising cytotoxicity against HCT-116, HepG-2, A-549, and MDA-MB-231 cells, with an $IC_{50}$ in the low micromolar range, via CDK-2 inhibition and apoptosis stimulation[18]. Thiophene carbohydrazide **III** displayed significant anticancer activity against CCRF, Panc-1, and HepG-2 cells by elevating CDKN1A, GDF-15, and DDIT4 and decreasing CDC-20, CDC-2, and CDK-2[19,20]. Furthermore, the tetrahydrobenzothienopyrimidine-containing hydrazine-1-carboxamide tail **IV** exhibited broad-spectrum anticancer activity against multiple NCI carcinomas and arrested the MCF-7 cell cycle[21,22]. Tetrahydrobenzo[*b*]thiophene carbamoyl analogue **V** showed a potent antitumor effect against HepG-2 cells, with an $IC_{50}$ in the low micromolar range, through CDK-2 inhibition and increased DNA fragmentation[28]. Besides, tetrahydrobenzo[*b*]thiophene acrylamide **VI** demonstrated potent cytotoxic and selective activity against the examined carcinomas, including HepG-2, MCF-7, and PC-3, with an $IC_{50}$ exceeding that of 5-fluorouracil by more than twofold[23]. Additionally, acrylamidotetrahydrobenzo[*b*]thiophene-3-carboxylate **VII** showed very potent inhibitory activity against HepG-2, MCF-7, and A-549 that may be assigned to the presence of the tetrahydro[*b*]benzothiophene-3-carboxylate scaffold (Figure 2).[24]

Guided by the previous data, new sets of tetrahydrobenzo[*b*]thiophene carboxamides **2–11** were designed using tetrahydrobenzo[*b*]thiophene carbamoyl analogue **V** by keeping the tetrahydrobenzo[*b*]thiophene scaffold and bioisosteric modifications that include chain contraction at C-2 position and substituent variations at C-3 position, to get new anticancer agents with CDK-2 inhibitory activity (Figure 3). All the prepared analogues were estimated against HepG-2, breast MCF-7, and MDA-MB-231 cells. The superior analogues were selected for the CDK-2 inhibition assay. The potent derivative was also assessed in apoptosis and cell cycle analysis. Also, DFT and molecular docking were used to identify a valid approach to optimising anticancer medications.

## Materials and methods

### *Conventional heating procedures*

The tools used to characterise the synthesised analogues are provided in the supplementary materials. Compound **1** was synthesised, and its X-ray crystallography was reported earlier[25].

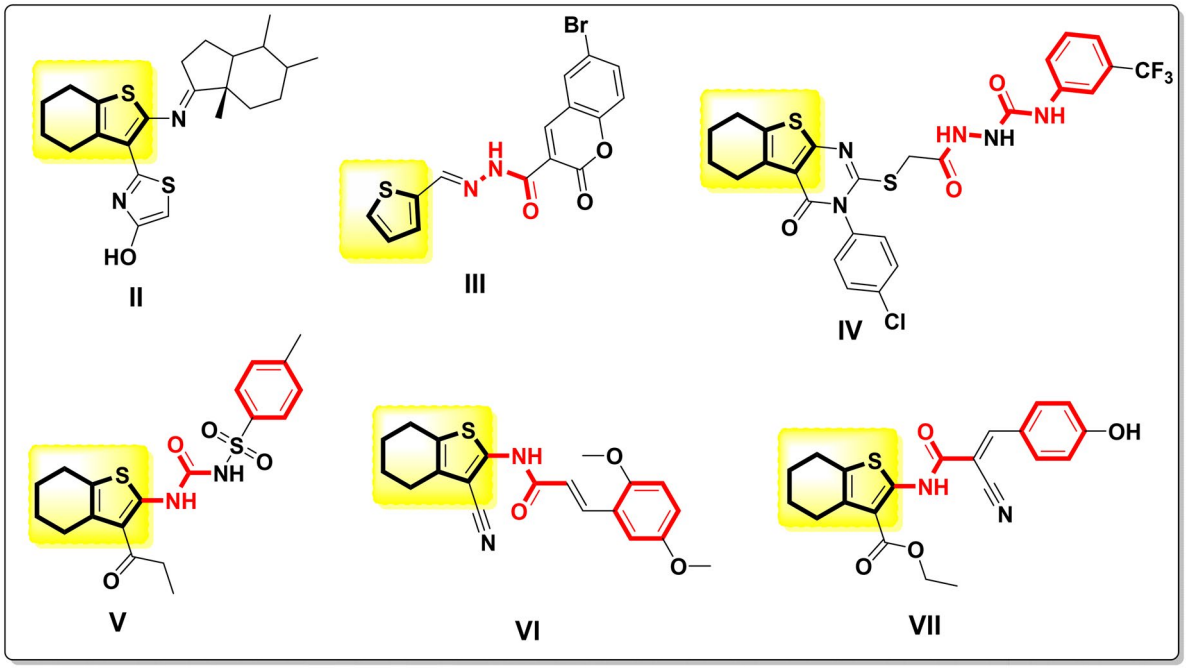


**Figure 2.** Reported thiophene and tetrahydrobenzo[*b*]thiophene as promising anticancer agents and CDK-2 inhibitors.

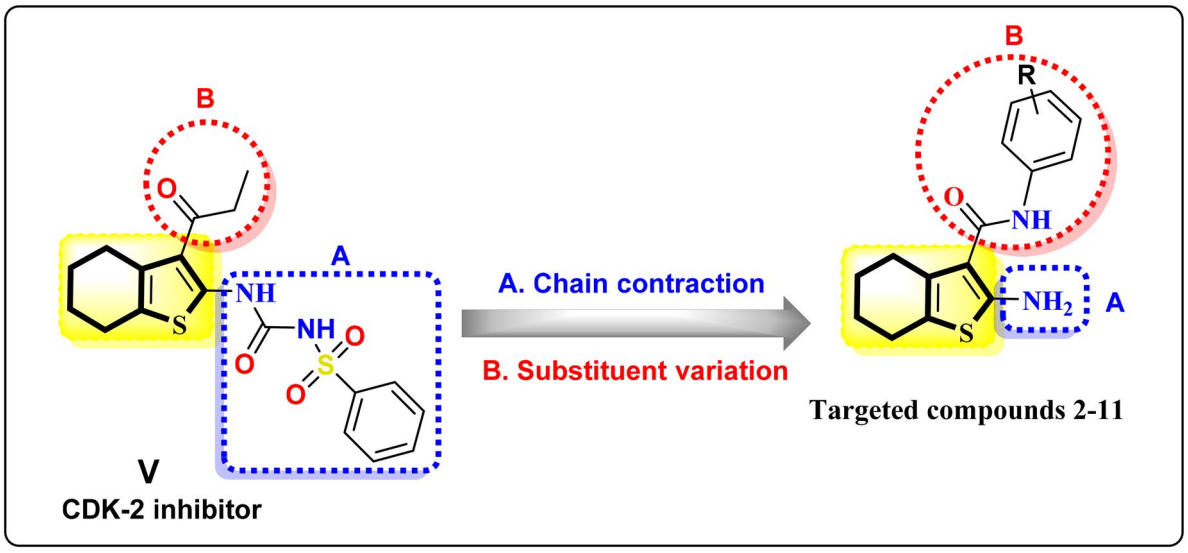


**Figure 3.** Design of tetrahydrobenzo[*b*]thiophene carboxamide candidates **2**–**11**.

### *General procedure for the synthesis of 4,5,6,7-tetrahydrobenzo[b]thiophenes (2–6)*

A solution of entity **1** (2.25 g, 0.01 mol) in acetone (15 ml) was refluxed for 4–16 h with each of *p*-phenylenediamine (1.08 g, 0.01 mol), *m*-phenylenediamine (1.08 g, 0.01 mol), benzidine (1.84 g, 0.01 mol), *o*-dianisidine (2.44 g, 0.01 mol), and 3,3′-dimethylbenzidine (2.12 g, 0.01 mol). Upon cooling, the solid was filtered, washed three times with ethanol (50 ml), and recrystallised from a suitable solvent to yield analogues **2–6**, respectively.

***2-Amino-N-(4-aminophenyl)-4,5,6,7-tetrahydrobenzo[b]thiophene-3-carboxamide (2).*** Grey crystals; recrystallised from methanol, m.p.: 182–184 °C. IR (KBr) $\upsilon$ cm$^{-1}$: 3402, 3297, 3231 ($NH_2$), 3168 (NH), 1646 (C=O), 1596, 1575 (C=C). $^1$H NMR (DMSO-$d_6$) $\delta$ (ppm): 1.60–1.77 (m, 4H, tetrahydrobenzothiophene-$C_{5,6}$-$CH_2$), 2.39–2.45 (m, 2H, tetrahydrobenzothiophene-$C_4$-$CH_2$), 2.59–2.65 (m, 2H, tetrahydrobenzothiophene-$C_7$-$CH_2$), 6.13 (s, 2H, $NH_2$, $D_2O$ exchangeable), 7.23 (d, 2H, $J$ = 8 Hz, $C_6H_4$-$C_{3,5}$-H), 7.68 (d, 2H, $J$ = 8 Hz, $C_6H_4$-$C_{2,6}$-H), 8.32 (s, 2H, $NH_2$, $D_2O$ exchangeable), 9.51 (s, 1H, NH, $D_2O$ exchangeable). $^{13}$C NMR (DMSO-$d_6$) $\delta$ (ppm): 22.9, 23.3, 24.1, 24.4, 115.8, 121.7, 121.8, 122.1, 125.5, 128.7, 131.6, 137.7, 149.1, 149.6, 163.2. MS: 287 *m/z* (29.24%). Anal. Calcd for $C_{15}H_{17}N_3OS$ (287): C, 62.69; H, 5.96; N, 14.62; S, 11.16. Found: C, 62.68; H, 6.01; N, 14.59; S, 11.23.

***2-Amino-N-(3-aminophenyl)-4,5,6,7-tetrahydrobenzo[b]thiophene-3-carboxamide (3).*** Black crystals; recrystallised from acetone, m.p.: 156–158 °C. IR (KBr) $\upsilon$ cm$^{-1}$: 3402, 3296 ($NH_2$), 3168 (NH), 1682 (C=O), 1640, 1595, 1575 (C=C). $^1$H NMR (DMSO-$d_6$) $\delta$ (ppm): 1.55–1.73 (m, 4H, tetrahydrobenzothiophene-$C_{5,6}$-$CH_2$), 2.40–2.49 (m, 2H, tetrahydrobenzothiophene-$C_4$-$CH_2$), 2.55–2.68 (m, 2H, tetrahydrobenzothiophene-$C_7$-$CH_2$), 5.20 (s, 2H, $NH_2$, $D_2O$ exchangeable), 6.52–6.70 (m, 2H, $C_6H_4$-$C_{2,4}$-H), 7.17–7.40 (m, 2H, $C_6H_4$-$C_{5,6}$-H), 8.32 (s, 2H, $NH_2$, $D_2O$ exchangeable), 10.20 (s, 1H, NH, $D_2O$ exchangeable). $^{13}$C NMR (DMSO-$d_6$) $\delta$ (ppm): 22.9, 23.3, 24.4, 27.0, 115.8 (2C), 117.1, 121.2, 125.4, 128.7, 131.6, 141.7, 156.0, 162.8, 165.9. MS: 287 *m/z* (9.98%). Anal. Calcd for $C_{15}H_{17}N_3OS$ (287): C, 62.69; H, 5.96; N, 14.62; S, 11.16. Found: C, 62.79; H, 5.87; N, 14.71; S, 11.09.

***2-Amino-N-(4′-amino-[1,1′-biphenyl]-4-yl)-4,5,6,7-tetrahydrobenzo[b]thiophene-3-carboxamide (4).*** Brown crystals; recrystallised from ethanol, m.p.: 142–144 °C. IR (KBr) $\upsilon$ cm$^{-1}$: 3402, 3296, 3225 ($NH_2$), 3168 (NH), 1702 (C=O), 1646, 1596, 1575 (C=C). $^1$H NMR (DMSO-$d_6$) $\delta$ (ppm): 1.55–1.80 (m, 4H, tetrahydrobenzothiophene-$C_{5,6}$-$CH_2$), 2.70–2.80 (m, 2H, tetrahydrobenzothiophene-$C_4$-$CH_2$), 2.85–2.95 (m, 2H, tetrahydrobenzothiophene-$C_7$-$CH_2$), 5.01 (s, 2H, $NH_2$, $D_2O$ exchangeable), 7.21–7.70 (m, 2H, $C_6H_4$-$C_{3',5'}$-H), 6.59–6.66 (m, 6H, $C_6H_4$-$C_{2',6'}$-H & $C_6H_4$-$C_{2,3,5,6}$-H), 7.97 (s, 2H, $NH_2$, $D_2O$ exchangeable), 8.01 (s, 1H, NH, $D_2O$ exchangeable). $^{13}$C NMR (DMSO-$d_6$) $\delta$ (ppm): 22.9, 23.3, 24.4, 27.0, 114.8, 115.9, 120.0 (2C), 127.1, 127.3, 127.4, 127.5, 131.8, 136.6, 147.3, 148.6, 159.9, 162.8, 162.9, 163.4, 165.6. MS: 363 *m/z* (11.31%). Anal. Calcd for $C_{21}H_{21}N_3OS$ (363): C, 69.39; H, 5.82; N, 11.56; S, 8.82. Found: C, 69.40; H, 5.84; N, 11.66; S, 8.77.

***2-Amino-N-(4′-amino-3,3′-dimethoxy-[1,1′-biphenyl]-4-yl)-4,5,6,7-tetrahydrobenzo[b]thiophene-3-carboxamide (5).*** Off-white crystals; recrystallised from methanol, m.p.: 160–162 °C. IR (KBr) $\upsilon$ $cm^{-1}$: 3430, 3339, 3296, 3228 ($NH_2$), 3167 (NH), 1645 (C=O), 1595, 1574 (C=C). $^1H$ NMR (DMSO-$d_6$) $\delta$ (ppm): 1.60–1.75 (m, 4H, tetrahydrobenzothiophene-$C_{5,6}$-$CH_2$), 2.35–2.45 (m, 2H, tetrahydrobenzothiophene-$C_4$-$CH_2$), 2.58–2.70 (m, 2H, tetrahydrobenzothiophene-$C_7$-$CH_2$), 3.85 (s, 3H, $OCH_3$), 3.95 (s, 3H, $OCH_3$), 4.68 (s, 2H, $NH_2$, $D_2O$ exchangeable), 6.66–7.00 (m, 6H, Ar-H), 7.23 (s, 2H, $NH_2$, $D_2O$ exchangeable), 10.67 (s, 1H, NH, $D_2O$ exchangeable). $^{13}C$ NMR (DMSO-$d_6$) $\delta$ (ppm): 22.9, 23.3, 24.4, 27.0, 55.8, 56.3, 114.5, 115.9, 118.8, 121.0, 121.7, 121.9, 122.1, 125.5, 125.6, 130.2, 131.8, 136.5, 147.0, 147.1, 149.3, 160.3, 163.4. MS: 423 *m/z* (29.17%). Anal. Calcd for $C_{23}H_{25}N_3O_3S$ (423): C, 65.23; H, 5.95; N, 9.92; S, 7.57. Found: C, 65.19; H, 6.02; N, 9.87; S, 7.63.

***2-Amino-N-(4′-amino-3,3′-dimethyl-[1,1′-biphenyl]-4-yl)-4,5,6,7-tetrahydrobenzo[b]thiophene-3-carboxamide (6).*** Grey crystals; recrystallised from acetone, m.p.: 198–200 °C. IR (KBr) $\upsilon$ $cm^{-1}$: 3403, 3375, 3338, 3297 ($NH_2$), 3168 (NH), 1645 (C=O), 1626, 1596, 1574 (C=C). $^1H$ NMR (DMSO-$d_6$) $\delta$ (ppm): 1.65–1.82 (m, 4H, tetrahydrobenzothiophene-$C_{5,6}$-$CH_2$), 2.13 (s, 3H, $CH_3$), 2.28 (s, 3H, $CH_3$), 2.35–2.45 (m, 2H, tetrahydrobenzothiophene-$C_4$-$CH_2$), 2.55–2.70 (m, 2H, tetrahydrobenzothiophene-$C_7$-$CH_2$), 4.78 (s, 2H, $NH_2$, $D_2O$ exchangeable), 6.62–7.25 (2m, 6H, Ar-H), 7.77 (s, 2H, $NH_2$, $D_2O$ exchangeable), 10.39 (s, 1H, NH, $D_2O$ exchangeable). $^{13}C$ NMR (DMSO-$d_6$) $\delta$ (ppm): 18.1, 18.6, 22.9, 23.3, 24.4, 27.0, 115.9, 121.7, 121.8, 122.0, 122.1, 123.4, 123.6, 124.1, 124.9, 125.6, 127.7, 127.8, 128.4, 131.7, 145.2, 163.4, 165.6. MS: 391 *m/z* (36.51%). Anal. Calcd for $C_{23}H_{25}N_3OS$ (391): C, 70.56; H, 6.44; N, 10.73; S, 8.19. Found: C, 70.63; H, 6.42; N, 10.69; S, 8.18.

### *General method for the synthesis of 4,5,6,7-tetrahydrobenzo[b]thiophenes (7–11)*

A solution of entity **1** (4.51 g, 0.02 mol) in acetone (15 ml) was refluxed for 10–28 h with each of *p*-phenylenediamine (1.08 g, 0.01 mol), *m*-phenylenediamine (1.08 g, 0.01 mol), benzidine (1.84 g, 0.01 mol), *o*-dianisidine (2.44 g, 0.01 mol), and 3,3′-dimethylbenzidine (2.12 g, 0.01 mol). Upon cooling, the reaction mixture was poured onto cold $H_2O$ (50 ml). The resulting mass was filtered and recrystallised from the appropriate solvent to yield compounds **7–11**.

***N,N′-(1,4-phenylene)bis(2-amino-4,5,6,7-tetrahydrobenzo[b]thiophene-3-carboxamide) (7).*** Grey crystals; recrystallised from acetone, m.p.: 232–234 °C. IR (KBr) $\upsilon$ $cm^{-1}$: 3324, 3231 ($NH_2$), 3184, 3078 (NH), 1730, 1710 (C=O), 1645, 1595, 1575 (C=C). $^1H$ NMR (DMSO-$d_6$) $\delta$ (ppm): 1.58–1.78 (m, 8H, tetrahydrobenzothiophene-$C_{5,6}$-$4CH_2$), 2.37–2.47 (m, 4H, tetrahydrobenzothiophene-$C_4$-$2CH_2$), 2.55–2.65 (m, 4H, tetrahydrobenzothiophene-$C_7$-$2CH_2$), 7.23 (s, 4H, Ar-H), 8.51 (s, 4H, $2NH_2$, $D_2O$ exchangeable), 10.16 (s, 2H, 2NH, $D_2O$ exchangeable). $^{13}C$ NMR (DMSO-$d_6$) $\delta$ (ppm): 22.9 (2C), 23.3 (2C), 24.4 (2C), 27.0 (2C), 115.9 (2C), 122.0 (2C), 125.6 (2C), 129.2 (2C), 131.8 (2C), 137.8 (2C), 163.4 (2C), 165.6 (2C). MS: 466 *m/z* (11.53%). Anal. Calcd for $C_{24}H_{26}N_4O_2S_2$ (466): C, 61.78; H, 5.62; N, 12.01; S, 13.74. Found: C, 61.69; H, 5.67; N, 11.95; S, 13.81.

***N,N′-(1,3-phenylene)bis(2-amino-4,5,6,7-tetrahydrobenzo[b]thiophene-3-carboxamide) (8).*** Brown crystals; recrystallised from acetone, m.p.: 266–268 °C. IR (KBr) $\upsilon$ $cm^{-1}$: 3315, 3220 ($NH_2$), 3172, 3090 (NH), 1735, 1710 (C=O), 1640, 1590, 1574 (C=C). $^1H$ NMR (DMSO-$d_6$) $\delta$ (ppm): 1.57–1.77 (m, 8H, tetrahydrobenzothiophene-$C_{5,6}$-$4CH_2$), 2.32–2.42 (m, 4H, tetrahydrobenzothiophene-$C_4$-$2CH_2$), 2.54–2.65 (m, 4H, tetrahydrobenzothiophene-$C_7$-$2CH_2$), 7.21–7.70 (m, 8H, 4 Ar-H and $2NH_2$), 10.14 (s, 1H, NH, $D_2O$ exchangeable), 10.17 (s, 1H, NH, $D_2O$ exchangeable). $^{13}C$ NMR (DMSO-$d_6$) $\delta$ (ppm): 22.8 (2C), 23.3 (2C), 24.4 (2C), 27.0 (2C), 115.9 (2C), 121.7, 122.1 (2C), 126.8 (2C), 128.8, 137.8 (2C), 144.6 (2C), 159.9 (2C), 160.1 (2C). MS: 466 *m/z* (25.78%). Anal. Calcd for $C_{24}H_{26}N_4O_2S_2$ (466): C, 61.78; H, 5.62; N, 12.01; S, 13.74. Found: C, 61.81; H, 5.73; N, 12.12; S, 13.60.

***N,N′-([1,1′-biphenyl]-4,4′-diyl)bis(2-amino-4,5,6,7-tetrahydrobenzo[b]thiophene-3-carboxamide) (9).*** Grey crystals; recrystallised from butanol, m.p.: >300 °C. IR (KBr) $\upsilon$ $cm^{-1}$: 3440, 3393, 3350, 3295 ($NH_2$), 3227, 3168 (NH), 1755, 1707 (C=O), 1645, 1595, 1575 (C=C). $^1H$ NMR (DMSO-$d_6$) $\delta$ (ppm): 1.59–1.79 (m, 8H, tetrahydrobenzothiophene-$C_{5,6}$-$4CH_2$), 2.38–2.48 (m, 4H, tetrahydrobenzothiophene-$C_4$-$2CH_2$), 2.56–2.66 (m, 4H, tetrahydrobenzothiophene-$C_7$-$2CH_2$), 7.23 (s, 4H, $2NH_2$, $D_2O$ exchangeable), 7.33–7.69 (m, 8H, Ar-H), 11.20 (s, 2H, 2NH, $D_2O$ exchangeable). $^{13}C$ NMR (DMSO-$d_6$) $\delta$ (ppm): 22.9 (2C), 23.3 (2C), 24.4 (2C), 27.0 (2C), 120.0 (4C), 126.4 (2C), 127.3 (2C), 127.7 (4C), 131.8 (2C), 136.6 (2C), 148.6 (2C), 163.4 (2C), 165.6 (2C).

MS: 542 *m/z* (22.54%). Anal. Calcd for $C_{30}H_{30}N_4O_2S_2$ (542): C, 66.39; H, 5.57; N, 10.32; S, 11.81. Found: C, 66.38; H, 5.62; N, 10.29; S, 11.90.

***N,N′-(3,3′-dimethoxy-[1,1′-biphenyl]-4,4′-diyl)bis(2-amino-4,5,6,7-tetrahydrobenzo[b]thiophene-3-carboxamide) (10).*** Grey crystals; recrystallised from dioxane, m.p.: >300 °C. IR (KBr) $\upsilon$ $cm^{-1}$: 3426, 3365, 3297, 3229 ($NH_2$), 3168, 3077 (NH), 1674, 1656 (C═O), 1645, 1595, 1574 (C═C). $^1$H NMR (DMSO-$d_6$) $\delta$ (ppm): 1.56–1.77 (m, 8H, tetrahydrobenzothiophene-$C_{5,6}$-$4CH_2$), 2.36–2.47 (m, 4H, tetrahydrobenzothiophene-$C_4$-$2CH_2$), 2.55–2.66 (m, 4H, tetrahydrobenzothiophene-$C_7$-$2CH_2$), 4.13 (s, 6H, $2OCH_3$), 6.74 (s, 4H, $2NH_2$, $D_2O$ exchangeable), 7.23 (s, 2H, $C_6H_3$-$C_{2,2}$′-H), 7.83–7.90 (m, 4H, $C_6H_3$-$C_{5,5'\,,\,6,\,6'}$-H), 9.67 (s, 2H, 2NH, $D_2O$ exchangeable). $^{13}$C NMR (DMSO-$d_6$) $\delta$ (ppm): 22.9 (2C), 23.3 (2C), 24.4 (2C), 27.0 (2C), 59.6 (2C), 115.9 (2C), 119.7 (2C), 121.9 (2C), 128.2 (2C), 129.1 (2C), 130.4 (2C), 137.8 (2C), 140.6 (2C), 159.9 (2C), 162.8 (2C), 164.9 (2C). MS: 602 *m/z* (18.24%). Anal. Calcd for $C_{32}H_{34}N_4O_4S_2$ (602): C, 63.76; H, 5.69; N, 9.30; S, 10.64. Found: C, 63.81; H, 5.49; N, 9.21; S, 10.74.

***N,N′-(3,3′-dimethyl-[1,1′-biphenyl]-4,4′-diyl)bis(2-amino-4,5,6,7-tetrahydrobenzo[b]thiophene-3-carboxamide) (11).*** Off-white crystals; recrystallised from dioxane, m.p.: >300 °C. IR (KBr) $\upsilon$ $cm^{-1}$: 3462, 3400, 3347, 3285 ($NH_2$), 3230, 3168 (NH), 1683, 1665 (C═O), 1645, 1594, 1575 (C═C). $^1$H NMR (DMSO-$d_6$) $\delta$ (ppm): 1.58–1.79 (m, 8H, tetrahydrobenzothiophene-$C_{5,6}$-$4CH_2$), 2.14 (s, 6H, $2CH_3$), 2.35–2.46 (m, 4H, tetrahydrobenzothiophene-$C_4$-$2CH_2$), 2.54–2.66 (m, 4H, tetrahydrobenzothiophene-$C_7$-$2CH_2$), 6.59–7.70 (m, 10H, Ar-H and $2NH_2$, $D_2O$ exchangeable), 10.20 (s, 2H, 2NH, $D_2O$ exchangeable). $^{13}$C NMR (DMSO-$d_6$) $\delta$ (ppm): 18.4 (2C), 22.9 (2C), 23.3 (2C), 24.4 (2C), 27.0 (2C), 115.9 (2C), 123.3 (2C), 124.5 (2C), 126.8 (2C), 131.0 (2C), 131.8 (2C), 134.0 (2C), 144.6 (2C), 146.6 (2C), 163.4 (2C), 165.6 (2C). MS: 570 *m/z* (15.39%). Anal. Calcd for $C_{32}H_{34}N_4O_2S_2$ (570): C, 67.34; H, 6.00; N, 9.82; S, 11.23. Found: C, 67.21; H, 6.04; N, 9.84; S, 11.34.

## Microwave-aided protocol

The amounts of reactants and the synthetic procedure of the microwave-aided protocol are similar to the conventional heating technique, but without solvent. Thin-layer chromatography was applied to follow the reaction's progress. The products were washed with methanol three times and recrystallised with a suitable solvent. A microwave-aided protocol was performed in an Anton Paar Monowave 300 using "10 ml" borosilicate glass vials where the vial was irradiated at 120 °C under 2–5 bar pressure and 200–400 W power for 1.5–5 min with 750 rpm magnetic stirring rate. It was found that the end product of the same reaction was identical in TLC, m.p., and mixed m.p. in both techniques. Compared to the traditional heating method, the microwave method produced higher yields in less time.

## Biological evaluation

### Cytotoxicity assay

The examined cancer cells, hepatic HepG-2 and breast MCF-7 and MDA-MB-231, have been purchased from American Type Culture Collection (Manassas, VA). MTT technique was applied and the $IC_{50}$ was determined using a non-linear regression model in GraphPad Prism software (San Diego, CA). Doxorubicin and roscovitine were used as standards guided by the reported method[26].

### CDK-2 inhibition

CDK-2 kit was obtained from Biosciences (San Diego, CA) and Biovision (Mountain View, CA) and the $IC_{50}$ was detected after repeating the experiments three successive times according to the manufacturer's guidelines[27]. The detailed procedure was discussed in the supplementary materials.

### Apoptosis assay

Apoptosis assay using Annexin V-FITC/PI kit was applied by FACS Calibre flow cytometer on dealing with the potent compound **11** at three concentrations ($IC_{50}$ (*x*), 5*x* and 10*x*) following the recorded technique[29]. The detailed procedure was discussed in the supplementary materials.

### Cell cycle analysis

Analysis of MDA-MB-231 cycle was performed by FACS Calibur flow cytometer (Biosciences, San Jose, CA) on dealing with the potent compound **11** at three concentrations ($IC_{50}$ (*x*), 5*x* and 10*x*) according to the reported procedure[30]. The detailed procedure was discussed in the supplementary materials.

### In silico studies

***Molecular orbital computations.*** The theoretical molecular orbital calculations were carried out utilising (DFT/B3LYP) as in Gaussian 09W software. The energy optimised structures of the synthesised analogues were executed by the standard double zeta plus polarisation with 6–31G (d,p) basis set.

***Molecular docking analysis.*** It was performed utilising Molecular Operating Environment (MOE-Dock) software, version 2024.0601. The co-crystallised structure of CDK-2/cyclin A2 with its natural ligand, roscovitine (PDB code: 3DDQ) extracted from the Protein Data Bank was applied.

## Results and discussion

### Chemistry

The microwave-assisted technique is a significant, eco-friendly approach that has recently been employed in the synthesis of heterocycles[31–33]. The condensation of amines with esters was reported to yield the corresponding amides[32,34–38]. Hence, unimolecular and bimolecular condensation of ethyl 2-aminobenzo[*b*] thiophene-3-carboxylate **1** with appropriate diamines, including *p*-phenylenediamine, *m*-phenylenediamine, benzidine, *o*-dianisidine, and 3,3′-dimethylbenzidine, furnished the corresponding 4,5,6,7-tetrahydrobenzo[*b*] thiophene-3-carboxamides **2**–**11** as shown in Schemes 1 and 2.

The reactions were intended to proceed via nucleophilic addition of $NH_2$ to the ester carbonyl, with the removal of an ethanol moiety to afford carboxamides **2**–**11**. The structures of newly synthesised analogues were evidenced by NH and amidic C=O bands in IR spectra at 3230–3077 and 1755–1645 $cm^{-1}$, respectively. Meanwhile, $^1H$ NMR spectra presented the disappearance of triplet and quartette signals connected with the ethyl carboxylate protons in the starting compound. They exhibited two $D_2O$ exchangeable singlets in the range of 4.68–8.51 and 8.01–11.20 ppm attributed to $NH_2$ and NH. Additionally, compounds **5** and **10** presented singlets at 3.85–4.13 ppm corresponding to methoxy protons, while compounds **6** and **11** illustrated singlets at 2.13–2.28 ppm due to methyl protons.

The mentioned spectral data of compounds **2**–**6** were consistent with the proposed mono-carboxamide structures and did not indicate the presence of bis-amide products. High-performance liquid chromatography (HPLC) analysis of compounds **5**, **6**, and **11** emphasised the high purity of the prepared entities. They showed single sharp peaks with retention times ranging from 4.32 to 4.56 min, indicating acceptable chromatographic homogeneity. The purity percent were 98.7, 98.1, and 100 for entities **5**, **6**, and **11**, respectively.

### Comparison between microwave and conventional thermal methods

A comparison of the newly synthesised compounds prepared by microwave and conventional procedures was conducted with respect to yields and timeframes. Table 1 shows that although the molar concentrations of all reactants were identical in the traditional and microwave techniques, the reaction durations and product yields differed greatly. However, employing both traditional and microwave approaches, the yield economy (YE) was employed to assess synthetically differing efficiencies of the same reaction[39–41].

$$YE = \frac{\text{yield\%}}{\text{reaction time}(\text{min})}.$$

Reaction mass efficiency (RME), on the other hand, is a useful indicator of reaction efficiency and can be calculated using the following formula[42–44]:

$$\text{RME} = \frac{\text{wt of isolated product}}{\text{wt of reactants}}.$$

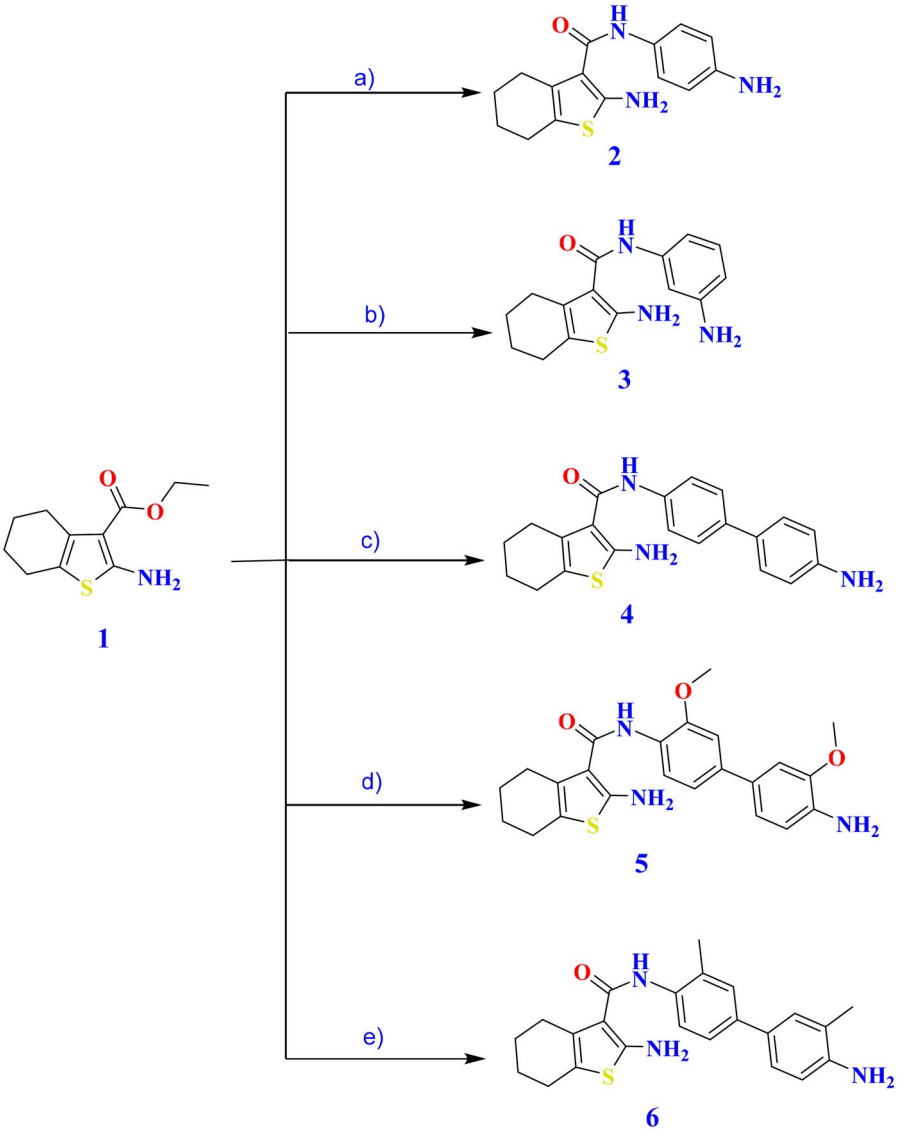


**Reagents and conditions**

a) *p*-phenylenediamine 1:1, acetone, reflux. b) *m*-phenylenediamine 1:1, acetone, reflux. c) benzidine 1:1, acetone, reflux. d) *o*-dianisidine 1:1, acetone, reflux. e) 3,3'-dimethylbenzidine 1:1, acetone, reflux.

**Scheme 1.** Synthesis of the targeted analogues **2**–**6**.

The two reaction types were directly compared using the optimal efficiency (OE), which may be computed using $OE = \frac{RME}{AE} \times 100$.

AE stands for "atomic economy." The AE is the same in both procedures used to synthesise the same target product, even though most parameters are larger in the microwave than in the conventional method[45,46]

## *Biological tests*

### *In vitro cytotoxicity study*

Using the MTT colorimetric method, the compounds' cytotoxicity was evaluated against three cancer cells, liver HepG-2, breast MCF-7, and MDA-MB-231. Based on their sensitivity to a pharmacophore-bearing tetrahydrobenzo[*b*]thiophene, the target carcinomas were chosen[25,47–49]. Additionally, the selected cancer cells are found to overexpress CDK-2[50,51]. Doxorubicin and roscovitine were used as references to assess

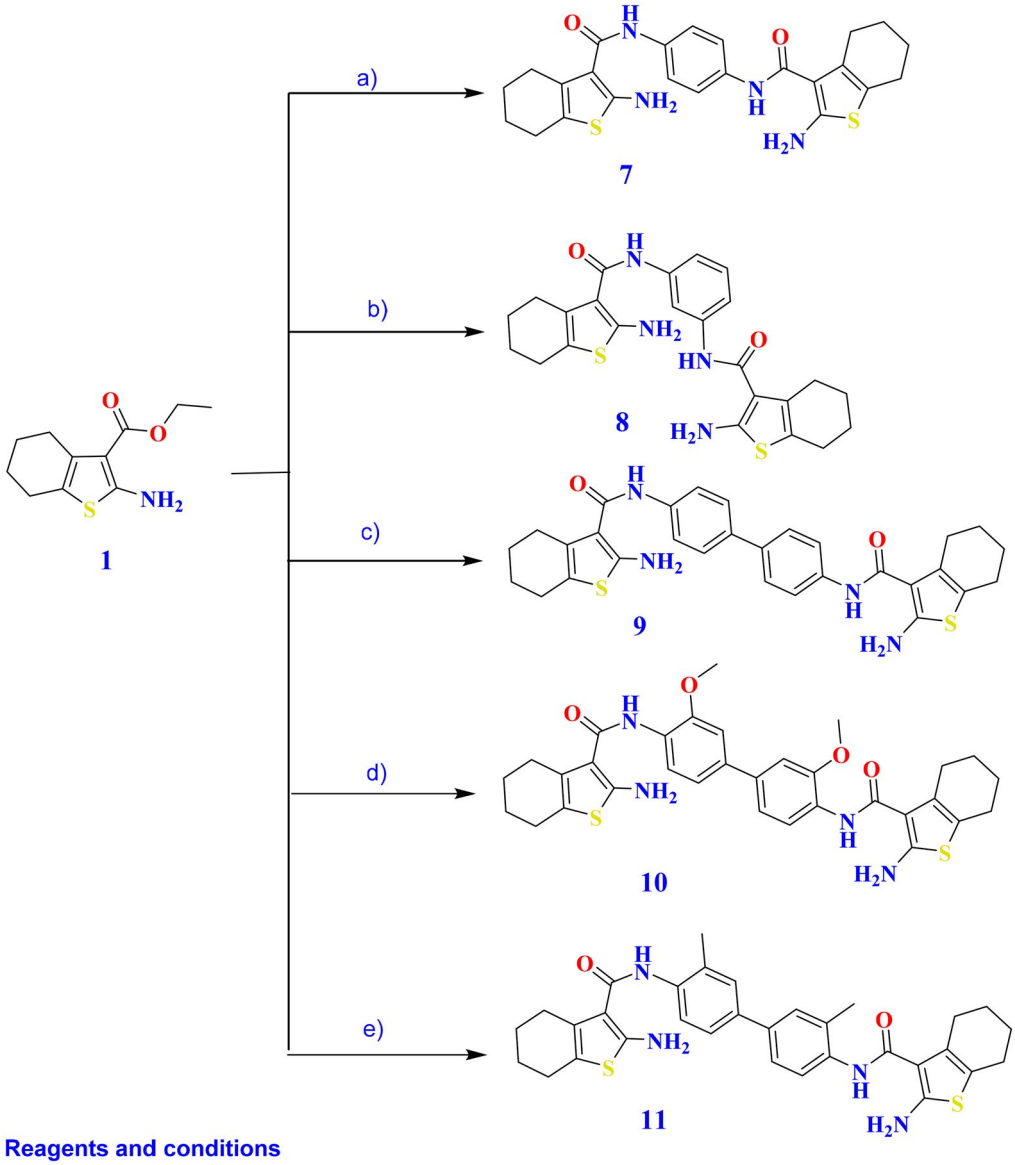


**Reagents and conditions**

a) *p*-phenylenediamine 1:2, acetone, reflux. b) *m*-phenylenediamine 1:2, acetone, reflux. c) benzidine 1:2, acetone, reflux. d) *o*-dianisidine 1:2, acetone, reflux. e) 3,3'-dimethylbenzidine 1:2, acetone, reflux.

**Scheme 2.** Synthesis of the target compounds **7**–**11**.

**Table 1.** Comparison of reaction efficiencies using conventional heating versus microwave-assisted synthesis.

| | Time (min) | | Yield % | | YE | | OE | | RME | | |
|---|---|---|---|---|---|---|---|---|---|---|---|
| Cpd. no. | Con. | M.W. | Con. | M.W. | Con. | M.W. | Con. | M.W. | Con. | M.W. | AE |
| **2** | 240 | 1.5 | 42 | 95 | 0.1750 | 63.33 | 36.213 | 81.91247 | 28.63 | 64.76 | 79.06 |
| **3** | 720 | 2.5 | 43 | 93 | 0.0597 | 37.20 | 37.07311 | 80.19226 | 29.31 | 63.40 | 79.06 |
| **4** | 480 | 2 | 41 | 92 | 0.0854 | 46.00 | 36.21962 | 81.26738 | 29.95 | 67.20 | 82.69 |
| **5** | 960 | 3 | 44 | 95 | 0.0458 | 31.67 | 39.94591 | 86.26099 | 29.54 | 63.79 | 73.95 |
| **6** | 840 | 4 | 42 | 91 | 0.0500 | 22.75 | 37.35818 | 80.93873 | 31.28 | 67.77 | 83.73 |
| **7** | 600 | 4 | 42 | 91 | 0.0700 | 22.75 | 37.55968 | 81.39257 | 28.32 | 61.37 | 75.40 |
| **8** | 900 | 4 | 41 | 92 | 0.0456 | 23.00 | 36.67109 | 82.28117 | 27.65 | 62.04 | 75.40 |
| **9** | 840 | 4.5 | 44 | 93 | 0.0524 | 20.67 | 39.80794 | 84.14853 | 31.09 | 65.72 | 78.10 |
| **10** | 1320 | 5 | 45 | 95 | 0.0341 | 19.00 | 41.35183 | 87.29221 | 30.10 | 63.54 | 72.79 |
| **11** | 1680 | 5 | 45 | 91 | 0.0268 | 18.20 | 40.8613 | 82.64725 | 32.26 | 65.25 | 78.95 |

Con.: conventional; M.W.: microwave.

the anticancer activity of the produced compounds. The findings in Table 2 demonstrate that tetrahydrobenzo[*b*]thiophene-3-carboxamides exhibit mild to extremely potent growth inhibition of the tested cancer cells. Compound **5** demonstrated the most potent cytotoxic effect, particularly against breast cancer cell lines, significantly surpassing doxorubicin. The reliability of these potency estimates was confirmed by the high goodness-of-fit ($R^2 \geq 0.94$) and the narrow 95% confidence intervals (CIs) for all tested compounds (detailed statistical parameters are provided in Table S1). The influence of structural variations on biological activity was systematically analysed to develop a clear structure–activity relationship (SAR) profile.

### *Structure–activity relationship*

Regarding monocarboxamide analogues **2–6**, compounds **2** and **3**, containing simple 4-aminophenyl and 3-aminophenyl substituents, respectively, demonstrated weak to moderate cytotoxicity ($IC_{50}$ values ranged from 47.3 to 82.27 µM). The slight improvement observed in compound **3** suggests that meta-amino substitution optimises geometric alignment for hydrogen bonding but remains insufficient for high activity. A significant improvement emerged upon introducing biphenyl-based anilide moieties (**4**–**6**). Compound **4**, featuring an unsubstituted biphenyl system, showed a substantial increase in potency ($IC_{50}$ = 8.24 µM on MDA-MB-231), confirming the beneficial role of extended aromatic systems in enhancing π–π stacking and hydrophobic interactions. Electron-donating substituents further modulated activity. The 3,3′-dimethoxy biphenyl analogue **5** displayed the highest potency in the entire series, with $IC_{50}$ values of 3.59 and 2.79 µM against MCF-7 and MDA-MB-231, respectively, surpassing doxorubicin on breast cancer cell lines. Replacing methoxy groups with methyl groups in compound **6** slightly reduced activity but maintained strong potency ($IC_{50}$s ranging from 9.50 to 11.93 µM), indicating that steric and hydrophobic effects contribute positively. However, the hydrogen-bonding properties of the methoxy group confer optimal activity.

On the other hand, bis-carboxamide analogues **7**–**11**, compounds with two tetrahydrobenzo[*b*]thiophene pharmacophores linked through aromatic spacers, activity varied depending on spacer geometry and electronic nature. The para-phenylene-linked bis-amide **7** showed moderate activity with $IC_{50}$ values ranging from 17.16 to 38.04 µM, surpassing the meta-phenylene analogue **8**, which had $IC_{50}$ values from 58.38 to 61.41 µM. This implies that a linear para-orientation enhances better molecular alignment and interaction with cellular targets. Introduction of biphenyl spacers **9**–**11** significantly restored biological activity. Among them, compound **11**, possessing 3,3′-dimethyl substituents, revealed the highest potency ($IC_{50}$s ranging from 5.61 to 6.88 µM in breast cancer lines). These results suggest that hydrophobicity and steric reinforcement improve binding affinity within the bis-series. The dimethoxy analogue **10** exhibited moderate potency, weaker than that of **11**, indicating that, in bis-amide structures, increased hydrophobic character is more influential than H-bonding capacity. A graphical presentation of SAR is summarised in Figure 4.

**Table 2.** *In vitro* cytotoxicity.

| | *In vitro* cytotoxicity $IC_{50}$ (µM)* | | |
|---|---|---|---|
| Analog number | MCF-7 | MDA-MB-231 | HepG-2 |
| **2** | 70.74 ± 3.7 ***, $$$ | 62.41 ± 3.5 ***, $$$ | 82.27 ± 4.1 ***, $$$ |
| **3** | 47.30 ± 2.8 ***, $$$ | 41.60 ± 2.4 ***, $$$ | 55.77 ± 3.2 ***, $$$ |
| **4** | 15.26 ± 1.2 ***, $$ | 8.24 ± 0.5 | 42.19 ± 2.4 ***, $$$ |
| **5** | 3.59 ± 0.2 | 2.79 ± 0.1 | 6.49 ± 0.4 |
| **6** | 9.50 ± 0.7 | 11.93 ± 0.8 *** | 8.74 ± 0.6 |
| **7** | 29.05 ± 1.9 ***, $$$ | 17.16 ± 1.3 ***, $$$ | 38.04 ± 2.3 ***, $$$ |
| **8** | 61.41 ± 3.4 ***, $$$ | 58.38 ± 3.3 ***, $$$ | 30.63 ± 2.1 ***, $$$ |
| **9** | 36.18 ± 2.2 ***, $$$ | 33.01 ± 2.0 ***, $$$ | 64.90 ± 3.5 ***, $$$ |
| **10** | 22.82 ± 1.5 ***, $$$ | 24.58 ± 1.6 ***, $$$ | 18.28 ± 1.4 ***, $$ |
| **11** | 6.88 ± 0.5 | 5.61 ± 0.3 | 21.51 ± 1.7 ***, $$$ |
| **Doxorubicin** | 4.17 ± 0.2 | 3.18 ± 0.1 | 4.50 ± 0.2 |
| **Roscovitine** | 7.26 ± 0.3 | 7.64 ± 0.4 | 9.18 ± 0.6 |

*The findings are the mean of 3 independent biological replicates ± SD. The cancer cells were treated with the prepared analogs at concentrations of 100, 50, 25, 12.5, 6.25, 3.125, and 1.56 µM and incubated for 24 h.

The statistical significance was assessed by one-way ANOVA followed by Tukey post-hoc test. GraphPad InStat (version 3.06) was used for analysis.

***Significantly different from doxorubicin at $p < 0.001$.

$$$ and $$: significantly different from roscovitine at $p < 0.001$ and $p < 0.01$, respectively.

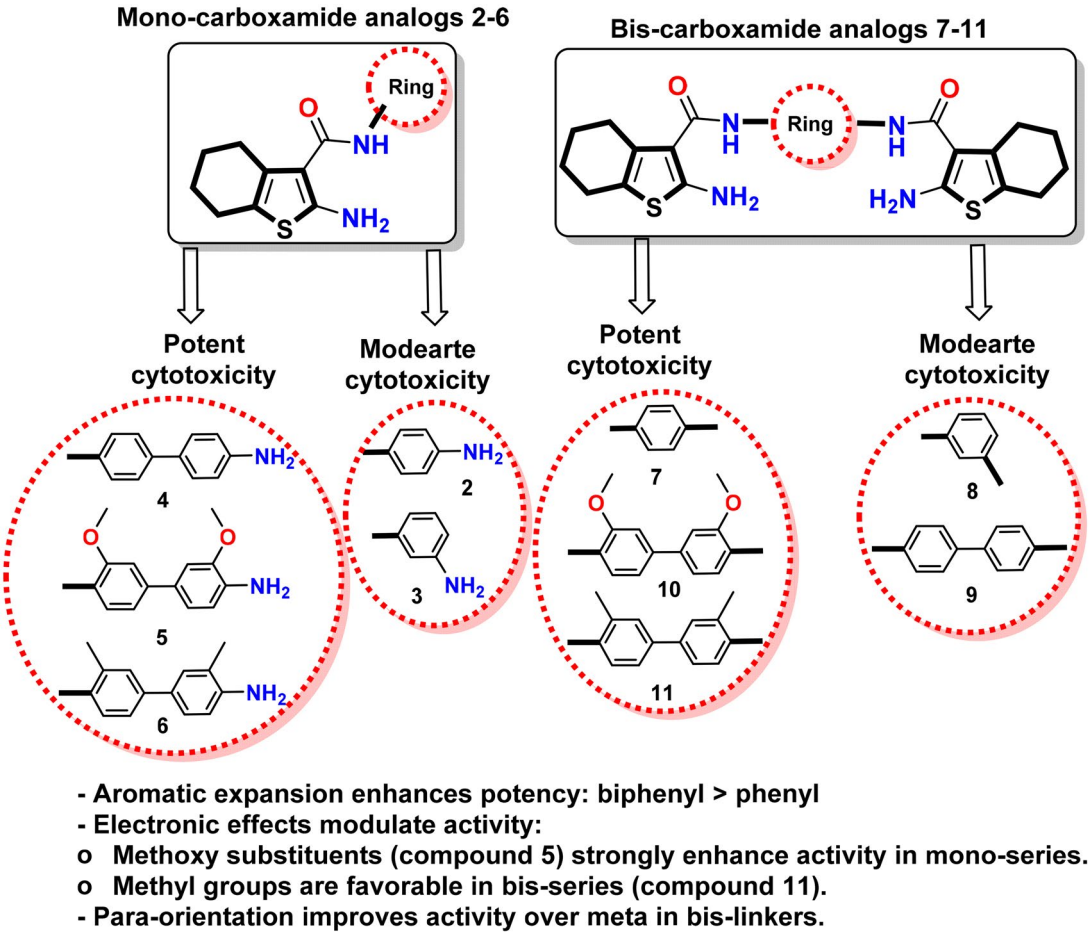


**Figure 4.** Graphical presentation of SAR.

The previous outcomes confirm that biphenyl-based tetrahydrobenzo[*b*]thiophene carboxamides, particularly those bearing electron-rich substituents, represent promising anticancer candidates. Compound **5** is the standout analogue with excellent potency, while compound **11** demonstrates the optimal design for bis-carboxamide derivatives.

### *Calculation of selectivity indices*

A compound's selectivity index (SI) is determined by dividing its $IC_{50}$ against a normal cell by that of a malignant cell[52–55]. To verify the selectivity of these candidates towards cancer cells, the cytotoxicity of the strongest anticancer compounds, **4**, **5**, **6**, and **11**, against WI-38 cells was measured. According to the results, they showed encouraging selectivity for the studied carcinomas (SI range of 1.37–12.71) compared with the references, roscovitine and doxorubicin (SI range of 1.16–2.11). Moreover, the superior cytotoxic analogue **5**, with dimethoxybiphenyltetrahydrobenzo[*b*]thiophene-3-carboxamide, exhibited the greatest selectivity towards MCF-7, MDA-MB-231, and HepG-2 cells, with SI values of 9.87, 12.71, and 5.46, respectively. Also, compound **6**, containing dimethylbiphenyltetrahydrobenzo[*b*]thiophene-3-carboxamide scaffold, displayed significant selectivity towards MCF-7, MDA-MB-231, and HepG-2 carcinomas with SI of 7.50, 5.97, and 8.15, respectively. Additionally, compound **11**, having dimethylbiphenylbis(tetrahydrobenzo[*b*]thiophene-3-carboxamide), exhibited significant selectivity against breast MCF-7 and MDA-MB-231 cells (SI = 7.63 and 9.36, respectively) and moderate selectivity against HepG-2 (SI = 2.44). However, compound **4**, with biphenyltetrahydrobenzo[*b*]thiophene-3-carboxamide, exhibited potent selectivity against MDA-MB-231 (SI = 7.02) and modest selectivity towards MCF-7 (SI = 3.79) with no selectivity against HepG-2 cells. Concerning cancerous cells, the order of selectivity of the synthesised analogues towards the tested carcinomas is MDA-MB-231 > MCF-7 > HepG-2. Meanwhile, the strongest cytotoxic and selective compound against the examined cancer cells is compound **5**, followed by **6** and **11**, with compound **4** coming last (Table 3).

### CDK-2 inhibition

CDK-2 overexpression correlates with the advancement of multiple types of malignancy, such as hepatic and breast tumours[56]. CDK is a prime option for pharmacological treatments in cancer therapy because of its broad function in proliferation[50]. The most effective and selective entities, **5**, **6**, and **11**, were selected for further testing to elucidate their molecular pathways based on the cytotoxicity assessment results. Consequently, the inhibition of CDK-2 was assessed for these compounds using roscovitine as a standard CDK-2 inhibitor. Compound **11**, containing dimethylbiphenylbis(tetrahydrobenzo[*b*]thiophene-3-carboxamide), exhibited the highest CDK-2 inhibition with an $IC_{50}$ of 0.096 µM that exceeded roscovitine by nearly threefold. Furthermore, dimethoxybiphenyltetrahydrobenzo[*b*]thiophene-3-carboxamide **5** displayed promising CDK-2 inhibition with an $IC_{50}$ of 0.245 µM, which is nearly identical to that of roscovitine (Table 4). Moreover, dimethylbiphenyltetrahydrobenzo[*b*]thiophene-3-carboxamide **6** showed a considerable CDK-2 inhibition with an $IC_{50}$ of 0.852 µM.

From previous data, bis-carboxamide architecture in **11** exhibited the most potent CDK-2 inhibition, which could enable additional hydrogen-bonding interactions within the hinge region and enhanced occupancy of the ATP-binding cleft. However, compound **5** (with dimethoxy groups) displayed stronger CDK-2 inhibition than compound **6** (with dimethyl ones), as methoxy groups could provide electron density and potentially stabilise ligand–enzyme interactions.

### Apoptosis induction

Apoptosis is a programmed form of cell death that occurs during normal cell proliferation and is induced by antitumor drugs. Many anticancer medications induce apoptosis as a crucial mechanism of action. In this study, compound **11**, the most potent CDK-2 inhibitor, was selected for further investigation to confirm its mechanism by assessing apoptosis in the most sensitive carcinoma, MDA-MB-231 cells, using the annexin V procedure[29]. The results demonstrated a distinct increase in both early and late apoptosis in MDA-MB-231 cells treated with compound **11**, with cellular percentages 12.02- and 64.48-fold higher than control, respectively (Figure 5 and Table S1). Also, the percentage of necrosis was elevated somewhat, exceeding the control by nearly 1.72-fold. Consequently, **11** was supposed to exert its activity through apoptosis induction (Figure 6).

**Table 3.** Selectivity indices of the superior compounds.

| | Cytotoxicity against WI-38 $IC_{50}$[a] (µM) ± SD | Selectivity index (SI)[b] | | |
|---|---|---|---|---|
| Compound's number | WI-38 | MCF-7 | MDA-MB-231 | HepG-2 |
| **4** | 57.88 ± 3.2*** | 3.79 | 7.02 | 1.37 |
| **5** | 35.45 ± 2.2*** | 9.87 | 12.71 | 5.46 |
| **6** | 71.22 ± 3.7*** | 7.50 | 5.97 | 8.15 |
| **11** | 52.52 ± 2.9*** | 7.63 | 9.36 | 2.44 |
| **Doxorubicin** | 6.72 ± 0.5 | 1.61 | 2.11 | 1.49 |
| **Roscovitine** | 10.65 ± 0.8 | 1.47 | 1.39 | 1.16 |

The statistical significance was assessed by one-way ANOVA followed by Tukey's post hoc test. GraphPad InStat (version 3.06) was used for analysis.
***Significantly different from doxorubicin or roscovitine at $p < 0.001$.
[a]$IC_{50}$ is the average ± SD of three experiments.
[b]SI: ≥5 (very selective), >2 (moderately selective), and <2 (not selective).

**Table 4.** CDK-2 inhibition.

| Compound number | $IC_{50}$ (µM) ± SD[a] |
|---|---|
| **5** | 0.245 ± 0.009 |
| **6** | 0.852 ± 0.031*** |
| **11** | 0.096 ± 0.003*** |
| **Roscovitine** | 0.288 ± 0.011 |

The statistical significance was assessed by one-way ANOVA followed by Tukey's post hoc test. GraphPad InStat (version 3.06) was used for analysis.
***Significantly different from roscovitine at $p < 0.001$.
[a]The data were computed following three consecutive experiments.

### *Cell cycle analysis*

CDK-2 regulates the G1/S and S/G2 phases, so its suppression is important for apoptosis induction and cell cycle arrest[57]. Herein, analogue **11** was selected to evaluate its impact on the MDA-MB-231 cell cycle to determine its mechanism. The outcomes showed that **11** increased cell accumulation in the G0/G1 phase to 71.39% compared with the control (51.84%). A concurrent increase was observed in this diminishment at the S and G2/M phases (Table 5). Hence, entity **11** induced apoptosis and arrested the cell cycle at the G0/G1 phase (Figure 7).

## *In silico studies*

### *Molecular orbital computation*

Geometry optimisations of compounds **2**–**11** were performed using the hybrid density functional theory (DFT) method at the B3LYP/6-31G(d,p) level as implemented in Gaussian 09W. The DFT calculations were carried out to obtain optimised ground-state geometries, frontier molecular orbital energies (HOMO and

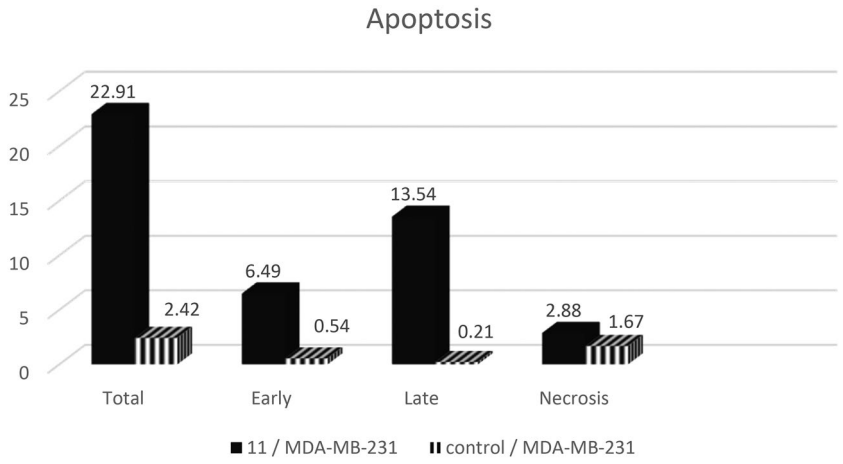


**Figure 5.** Apoptosis assay of **11**.

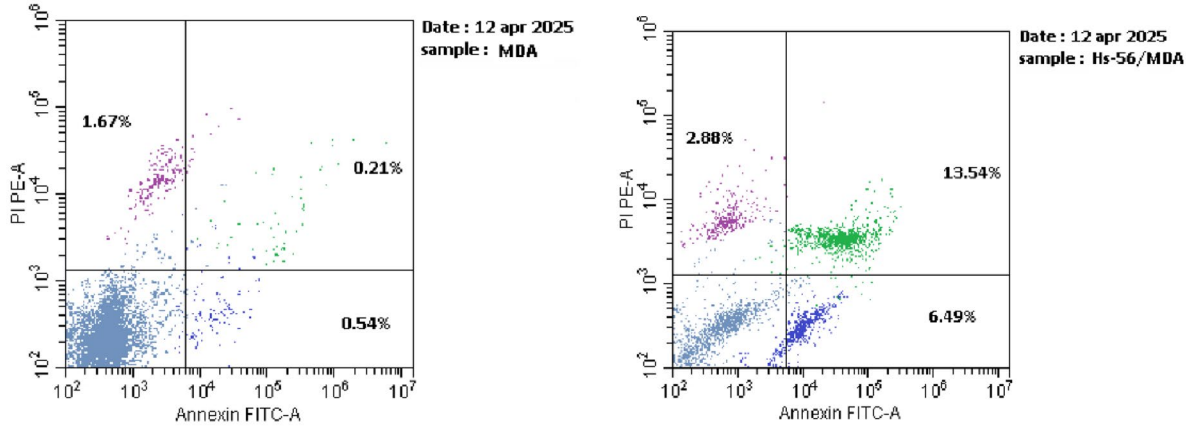


**Figure 6.** Apoptosis of MDA-MB-231 cells on treatment with control (at left) and **11** (at right). The lower left quadrants showed live cells (AV-negative/PI-negative), the lower right quadrants represented early apoptotic cells (AV-positive/PI-negative), the upper right quadrants showed late apoptotic cells or necrotic cells (AV-positive/PI-positive), and the upper left quadrants represented necrotic cells (AV-negative/PI-positive).

**Table 5.** Cell cycle analysis.

| Code | G0/G1 (%) | S phase (%) | G2/M (%) |
|---|---|---|---|
| **11** | 71.39 ± 4.23 | 21.57 ± 1.56 | 7.04 ± 0.61 |
| Control | 51.84 ± 2.75 | 34.18 ± 2.27 | 13.98 ± 1.14 |

LUMO), dipole moments, and global reactivity descriptors. The parent compound **1** had previously been characterised by single-crystal X-ray diffraction and DFT analysis[25].

Before DFT optimisation, preliminary conformational searches and geometry refinements were performed using molecular mechanics (MMFF94x force field). The energy values reported in Figures 8 and 9 (kcal/mol) correspond to MM minimisation energies and represent relative conformational strain within the same force-field framework. These values do not represent DFT total electronic energies and should not be interpreted as absolute thermodynamic stability indicators or compared across molecules of different sizes.

The DFT total energies reported in Table 6 (eV) correspond to raw electronic energies obtained from Gaussian calculations. As these energies scale with molecular size and electron count, they are not directly comparable between different derivatives and are reported only for completeness.

The optimised geometries reveal that compounds **2**–**7** adopt unsymmetrical conformations (*C1* point group). Intramolecular N–H···O hydrogen bonds were observed in several derivatives, with N–H···O distances ranging from 1.62 to 1.92 Å, supporting conformational stabilisation. In compounds **5** and **6**, the substituted biphenyl fragments adopt nearly perpendicular orientations relative to the parent core (dihedral angles of 88.1° and 76.3°, respectively), reflecting steric effects imposed by methoxy and methyl substituents. Compound **7** exhibits partial bending of one parent moiety towards the central phenyl ring (dihedral angle ≈35°), suggesting possible intramolecular π–π interactions.

## *Global reactivity descriptors*

Global reactivity descriptors were calculated from the DFT-derived *HOMO* and *LUMO* energies, including the energy gap (Δ*E*), electronegativity (*χ*), chemical potential (*V*), ionisation potential (*IP*), electron affinity

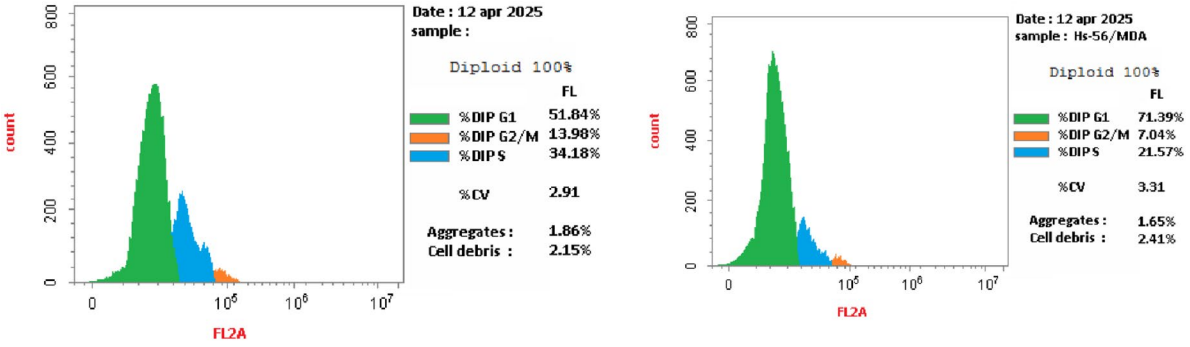


**Figure 7.** The effect of DMSO (left) and **11** (right) on MDA-MB-231 cell cycle.

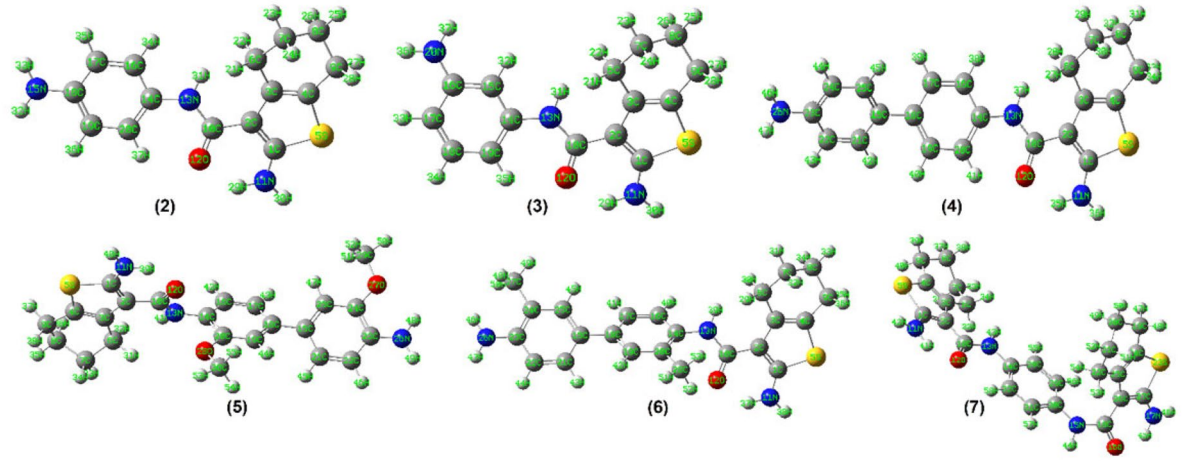


**Figure 8.** The energy optimised structures of **2**–**7**.

(*EA*), global hardness (*η*), softness (*S*), and electrophilicity index (*ω*). The *HOMO–LUMO* energy gap (Δ*E*) reflects electronic excitation energy and charge-transfer tendency rather than biological potency.

Among the studied compounds, derivative **9** exhibited the smallest Δ*E* value (2.18 eV), whereas the remaining derivatives showed Δ*E* values in the range of 4.07–4.49 eV. Compound **9** also displayed the highest *EA* (2.45 eV), lowest hardness (*η* = 1.09 eV), and highest electrophilicity index (*ω* = 5.74 eV), indicating increased electronic softness and charge-accepting capability (Table 6, Figures 10 and 11).

However, no direct quantitative correlation was observed between Δ*E*, electrophilicity index, or other global descriptors and the experimentally measured biological activity. Notably, although compound **9** reveals the highest electrophilicity and smallest energy gap, it is not among the most biologically active derivatives. This indicates that cytotoxic potency is governed by multiple factors, including target binding interactions, steric complementarity, and pharmacokinetic properties, rather than frontier orbital parameters alone. Therefore, the DFT descriptors are discussed here as indicators of intrinsic electronic properties and molecular reactivity trends, without implying predictive SARs.

## *Molecular docking analysis*

Molecular docking was applied to the most potent cytotoxic analogues, tetrahydrobenzo[*b*]thiophene carboxamides **5**, **6**, and **11**, to explain differences in their enzyme inhibitory activity and to justify their *in vitro* cytotoxicity. Docking simulations were carried out using the Molecular Operating Environment (MOE-Dock) software, version 2024.0601[58,59]. The co-crystallised structure of CDK-2/cyclin A2 with its natural ligand, roscovitine (PDB code: 3DDQ), has been deposited in the Protein Data Bank[60,61]. When the

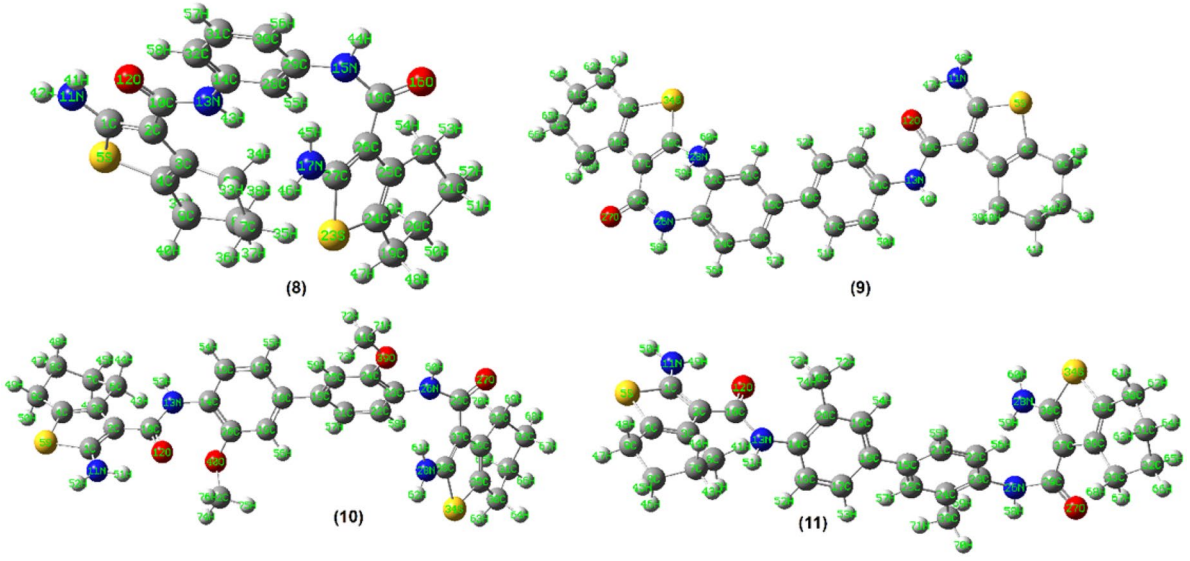


**Figure 9.** The energy optimised structures of **8**–**11**.

**Table 6.** The global chemical reactivity descriptors for the prepared analogues.

| Parameter | 1[a] | 2 | 3 | 4 | 5 | 6 | 7 | 8 | 9 | 10 | 11 |
|---|---|---|---|---|---|---|---|---|---|---|---|
| Total energy (eV) | −28 066 | −33 178 | −33 178 | −39 464 | −45 694 | −41 603 | −57 026 | −57 026 | −63 300 | −69 542 | −65 451 |
| *DM* (Debye) | 0.71 | 2.74 | 3.97 | 2.58 | 2.39 | 2.82 | 4.51 | 3.09 | 8.56 | 5.09 | 4.04 |
| *HOMO* (eV) | −5.16 | −4.64 | −4.95 | −4.77 | −4.73 | −4.84 | −5.00 | −5.20 | −4.63 | −5.08 | −5.13 |
| *LUMO* (eV) | −0.53 | −0.31 | −0.46 | −0.61 | −0.39 | −0.44 | −0.85 | −0.82 | −2.45 | −1.00 | −0.98 |
| Δ*E* (eV) | 4.63 | 4.33 | 4.49 | 4.16 | 4.34 | 4.40 | 4.14 | 4.38 | 2.18 | 4.07 | 4.15 |
| *X* (eV) | 2.85 | 2.47 | 2.71 | 2.69 | 2.56 | 2.64 | 2.93 | 3.01 | 3.54 | 3.04 | 3.06 |
| *V* (eV) | −2.85 | −2.47 | −2.71 | −2.69 | −2.56 | −2.64 | −2.93 | −3.01 | −3.54 | −3.04 | −3.06 |
| *EA* (eV) | 0.53 | 0.31 | 0.46 | 0.61 | 0.39 | 0.44 | 0.85 | 0.82 | 2.45 | 1.00 | 0.98 |
| *IP* (eV) | 5.16 | 4.64 | 4.95 | 4.77 | 4.73 | 4.84 | 5.00 | 5.20 | 4.63 | 5.08 | 5.13 |
| *η* (eV) | 2.31 | 2.17 | 2.24 | 2.08 | 2.17 | 2.20 | 2.07 | 2.19 | 1.09 | 2.04 | 2.08 |
| *S* (eV) | 1.16 | 1.08 | 1.12 | 1.04 | 1.09 | 1.10 | 1.04 | 1.09 | 0.55 | 1.02 | 1.04 |
| *ω* (eV) | 1.75 | 1.41 | 1.63 | 1.74 | 1.51 | 1.58 | 2.07 | 2.07 | 5.74 | 2.27 | 2.25 |

[a]Ref[25].

docking procedure was verified using the original ligand, energy scores of −11.26 kcal/mol and a low RMSD of 0.79 Å between the docked pose and the co-crystallised structure were obtained. Purine's H-bond interactions with **Glu81** and **Leu83** in the hinge region enabled roscovitine to fit into the CDK-2/cyclin A2 binding pocket, as reported[62]. Furthermore, the benzyl moiety established an arene-H contact with **Ile10**, whereas benzylamino showed further H-bonding with the **Leu83** backbone.

As depicted in Figures 12 and 13, with energy scores of −10.62, −8.19, and −11.18 kcal/mol, respectively, the screened tetrahydrobenzo[*b*]thiophene carboxamides **5**, **6**, and **11** were appropriately

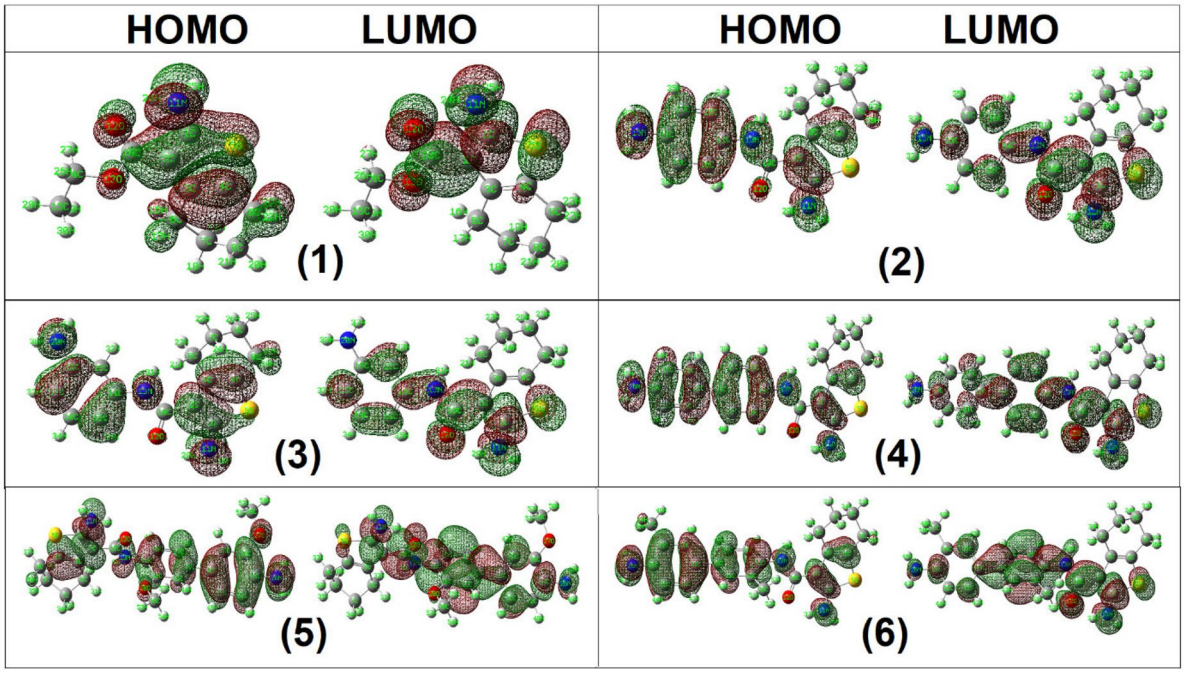


**Figure 10.** The frontier *HOMO* and *LUMO* orbitals of analogues **1**–**6**.

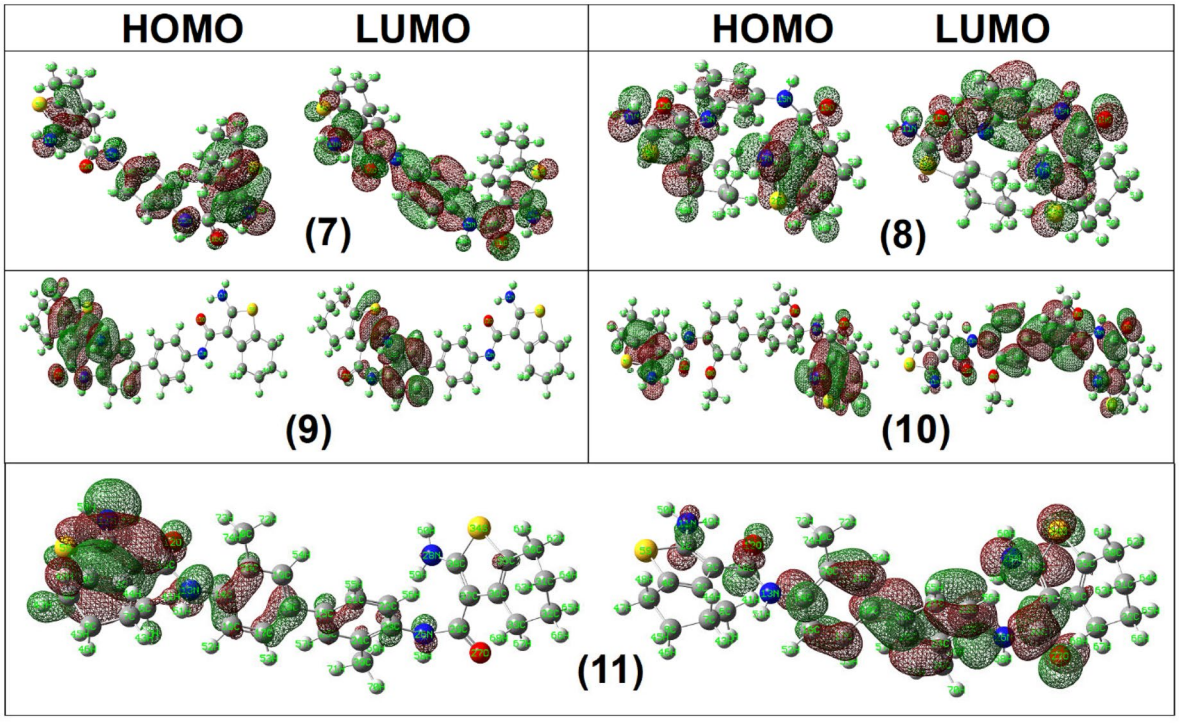


**Figure 11.** The frontier *HOMO* and *LUMO* orbitals of analogues **7**–**11**.

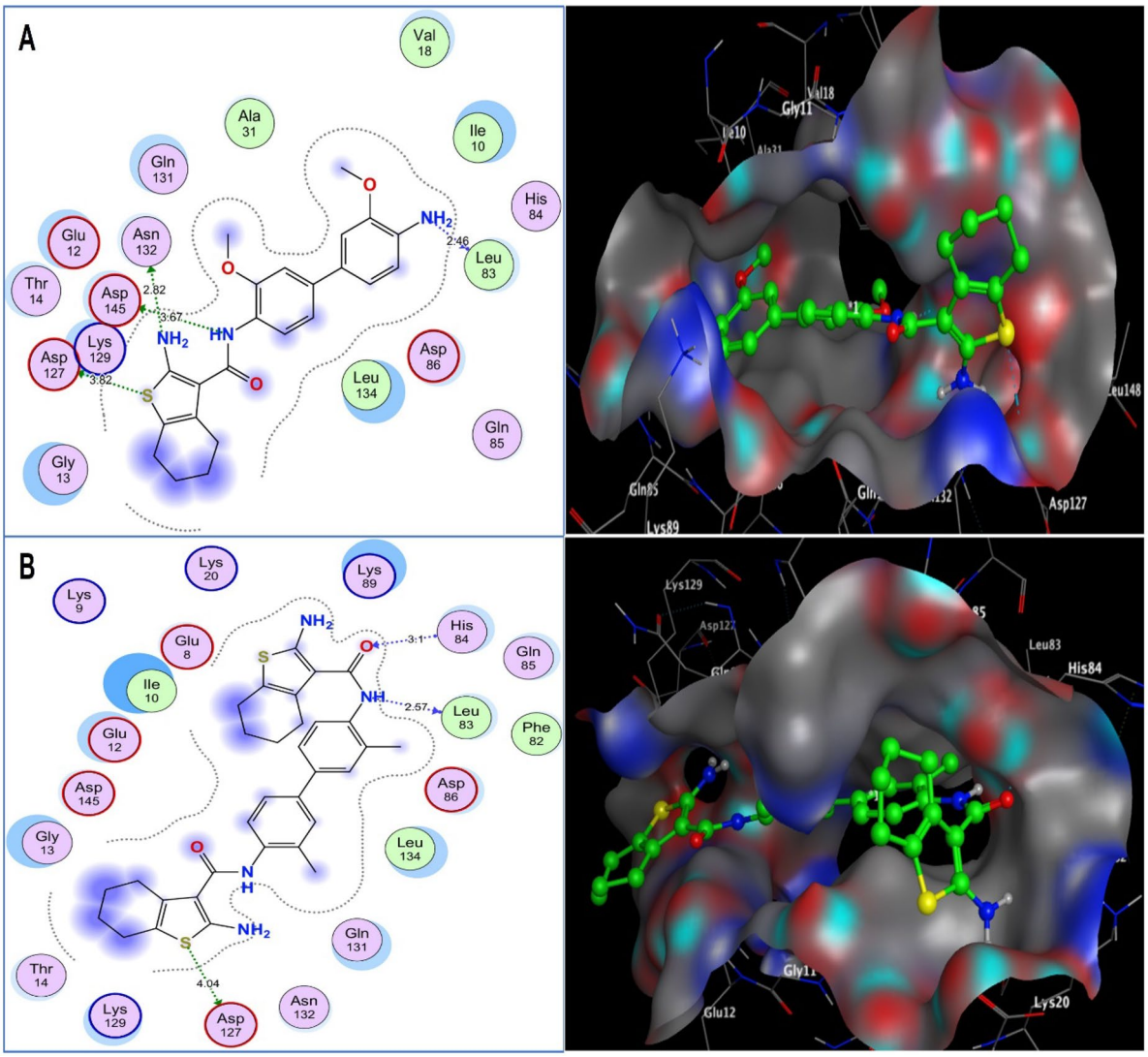


**Figure 12.** (A, B) Diagrams demonstrate two and three-dimensional views of the excellent tetrahydrobenzo[*b*]thiophene carboxamides **5** and **11** within CDK-2/cyclin A2 active site (PDB code: 3DDQ), respectively.

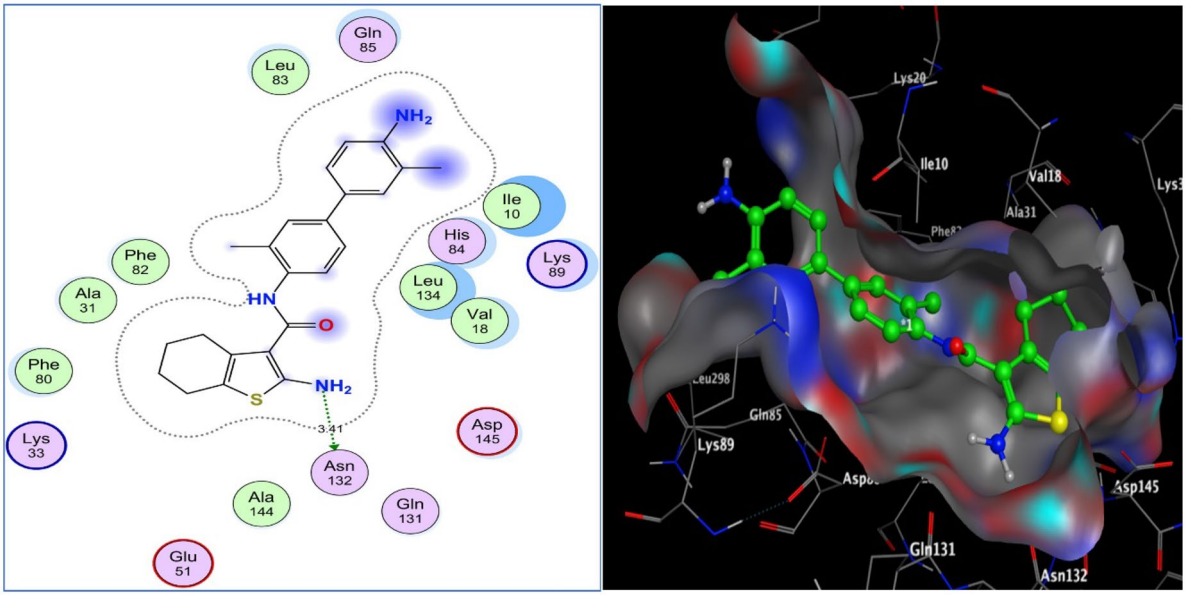


**Figure 13.** Two- and three-dimensional views of the weak tetrahydrobenzo[*b*]thiophene carboxamide **6** within CDK-2/cyclin A2 active site (PDB code: 3DDQ).

implemented in CDK-2/cyclin A2. Sulphur of thiophene in both **5** and **11** shared weak hydrogen bonds with the **Asp127** sidechain (distances: 3.82 and 4.04 Å, respectively). Nitrogens of the amino group at C-2 of tetrahydrobenzo[*b*]thiophene and the carboxamide in **5** donated two H-bonds with the sidechains of **Asn132** and **Asp145** (distances: 3.67 and 2.82 Å, respectively). Additionally, the **Leu83** backbone in the hinge region of CDK-2 displayed hydrogen bondin inhibitors in cancer therapy: an g with the nitrogens of the amino group at p-4 of the biphenyl moiety in **5** and the carboxamide fragment in the remaining part of the **11** molecule (distances: 2.46 and 2.57 Å, respectively), resembling roscovitine. Analogue **11** showed a further H-bond acceptor between the His84 backbone and the carboxamide oxygen (distance: 3.1 Å). On the other hand, the weak inhibitory analogue **6** revealed only one H-bond between the amino nitrogen at C-2 of tetrahydrobenzo[*b*]thiophene and the sidechain of **Asn132** (distance: 3.41 Å).

Among the investigated tetrahydrobenzo[*b*]thiophene-3-carboxamide analogues, **5** and **11** demonstrated superior inhibitory potency, attributed to the ability to form multiple stabilising hydrogen bonds with key CDK-2 residues, including **Asp127**, **Leu83**, and **His84** in **11** and additional hydrogen bonds with **Asn132** and **Asp145** in **5**. These interactions collectively strengthened their accommodation within the ATP-binding pocket, exceeding the binding efficiency of the reference drug roscovitine.

## Conclusions

Regarding the advancement of potential CDK-2 inhibitors, two sets of 4,5,6,7-tetrahydrobenzo[*b*]thiophene carboxamides were synthesised using conventional and eco-friendly microwave-aided procedures. These analogues were assessed for their antitumor effects against hepatic HepG-2 and breast MCF-7 and MDA-MB-231 carcinomas, in which dimethoxy **5** and dimethyl-bearing analogues **6** and **11** demonstrated significant cytotoxicity and selectivity against the examined cancer cells. Consequently, they were chosen for further assays to determine their mechanism. The findings suggest that these compounds may exert cytotoxicity by inhibiting CDK-2. Compound **11**, containing dimethylbiphenylbis(tetrahydrobenzo[*b*]thiophene-3-carboxamide), displayed the highest CDK-2 inhibition with an $IC_{50}$ of 0.096 µM that exceeded roscovitine by nearly threefold. Besides, it arrested the MDA-MB-231 cell cycle at the G0/G1 phase by apoptotic stimulation. Molecular modelling showed strong binding of the bioactive analogues to the active pocket of CDK-2 receptor, suggesting their potential as lead inhibitors.

## Acknowledgments

The authors extend their appreciation to Princess Nourah bint Abdulrahman University Researchers Supporting Project number (PNURSP2026R89), Princess Nourah bint Abdulrahman University, Riyadh, Saudi Arabia for funding this work.

The authors also acknowledge support from the KIT-Publication Fund of the Karlsruhe Institute of Technology.

## Author contributions

CRediT: **Kurls E. Anwer:** Writing – original draft, Visualization, Validation, Supervision, Resources, Methodology, Investigation, Formal analysis, Data curation, Conceptualization. **Ramadan M. Ramadan:** Writing – original draft, Visualization, Validation, Formal analysis, Conceptualization. **Eman S. Nossier:** Writing – review & editing, Validation, Software, Formal analysis, Data curation, Conceptualization. **Najla A. Altwaijry:** Writing – original draft, Validation, Resources, Investigation, Funding. **Asmaa Saleh:** Writing – original draft, Validation, Resources, Investigation, Formal analysis. **Stefan Bräse:** Writing – review & editing, Validation, Supervision, Funding, Resources. **Ebtehal M. Husseiny:** Writing – review & editing, Writing – original draft, Visualization, Validation, Supervision, Software, Resources, Methodology, Data curation, Conceptualization, Investigation.

## Disclosure statement

The authors report no conflicts of interest.

## Funding

This work was supported by Princess Nourah bint Abdulrahman University Researchers Supporting Project number (PNURSP2026R89) and Princess Nourah bint Abdulrahman University, Riyadh, Saudi Arabia. The authors also acknowledge support from the KIT-Publication Fund of the Karlsruhe Institute of Technology.

## ORCID

Kurls E. Anwer http://orcid.org/0000-0003-3017-8806
Ramadan M. Ramadan http://orcid.org/0000-0002-9755-5410
Ebtehal M. Husseiny http://orcid.org/0000-0001-6594-1766

## Data availability statement

The data that confirm the findings of this article are available in the supplementary material.

## References

1. Bray F, Laversanne M, Weiderpass E, Soerjomataram I. The ever-increasing importance of cancer as a leading cause of premature death worldwide. Cancer. 2021;127(16):3029–3030.
2. Shaker AMM, Shahin MI, AboulMagd AM, Abdel-Rahman HM, Ella DAAE. Design, synthesis, and molecular docking of novel 1,3,4-triaryl pyrazole derivatives bearing methylsulfonyl moiety with anticancer activity through dual targeting CDK2 and COX-2 enzymes. J Mol Struct. 2024;1301:137323.
3. Mignani S, Rodrigues J, Tomas H, Zablocka M, Shi X, Caminade A-M, Majoral J-P. Dendrimers in combination with natural products and analogues as anti-cancer agents. Chem Soc Rev. 2018;47(2):514–532.
4. Qayed WS, Hassan MA, El-Sayed WM, Rogério A, Silva J, Aboul-Fadl T. Novel azine linked hybrids of 2-indolinone and thiazolidinone scaffolds as CDK2 inhibitors with potential anticancer activity: in silico design, synthesis, biological, molecular dynamics and binding free energy studies. Bioorg Chem. 2022;126:105884.
5. Azmy EM, Hagras M, Ewida MA, Doghish AS, Gamil Khidr E, El-Husseiny AA, Gomaa MH, Refaat HM, Ismail NSM, Nassar IF, et al. Development of pyrolo[2,3-c]pyrazole, pyrolo[2,3-d]pyrimidine and their bioisosteres as novel CDK2 inhibitors with potent in vitro apoptotic anti-proliferative activity: synthesis, biological evaluation and molecular dynamics investigations. Bioorg Chem. 2023;139:106729.
6. Shah A, Teraiya N, Kamdar JH, Juneja T, Sangani CB, Ahmed S, Kapadiya K. Novel purine derivatives as selective CDK2 inhibitors with potential anticancer activities: design, synthesis and biological evaluation. Bioorg Chem. 2024;153:107841.
7. Cheng W, Yang Z, Wang S, Li Y, Wei H, Tian X, Kan Q. Recent development of CDK inhibitors: an overview of CDK/inhibitor co-crystal structures. Eur J Med Chem. 2019;164:615–639.
8. Marak BN, Dowarah J, Khiangte L, Singh VP. A comprehensive insight on the recent development of cyclic dependent kinase inhibitors as anticancer agents. Eur J Med Chem. 2020;203:112571.
9. Zhang Y, Liu X, Li Z, Wang X, Tang C. Development of 9H-purine scaffold as novel CDK2 inhibitors: design, synthesis, and biological evaluation. Bioorg Med Chem Lett. 2025;122:130166.
10. Akli S, Van Pelt CS, Bui T, Meijer L, Keyomarsi K. Cdk2 is required for breast cancer mediated by the low-molecular-weight isoform of cyclin E. Cancer Res. 2011;71(9):3377–3386.
11. Tadesse S, Caldon EC, Tilley W, Wang S. Cyclin-dependent kinase 2 inhibitors in cancer therapy: an update. J Med Chem. 2019;62(9):4233–4251.
12. Wang X, Chen X, Han W, Ruan A, Chen L, Wang R, Xu Z, Xiao P, Lu X, Zhao Y, et al. MiR-200c targets CDK2 and suppresses tumorigenesis in renal cell carcinoma. Mol Cancer Res. 2015;13(12):1567–1577.
13. Yang L, Fang D, Chen H, Lu Y, Dong Z, Ding H-F, Jing Q, Su S-B, Huang S. Cyclin-dependent kinase 2 is an ideal target for ovary tumors with elevated cyclin E1 expression. Oncotarget. 2015;6(25):20801–20812.
14. Yin X, Yu J, Zhou Y, Wang C, Jiao Z, Qian Z, Sun H, Chen B. Identification of CDK2 as a novel target in treatment of prostate cancer. Future Oncol. 2018;14(8):709–718.
15. Tong J, Tan X, Hao S, Ermine K, Lu X, Liu Z, Jha A, Yu J, Zhang L. Inhibition of multiple CDKs potentiates colon cancer chemotherapy via P73-mediated DR5 induction. Oncogene. 2023;42(12):869–880.
16. Younes A, Shawer T, El-Sehrawi H. Design, synthesis and antiproliferative evaluation of novel pyrazolo-pyrimidine derivatives with expected cyclin-dependent kinase 2 inhibitory effect. Azhar Int J Pharm Med Sci. 2022;2(2):9–20.
17. Wang Y, Chen Y, Cheng X, Zhang K, Wang H, Liu B, Wang J. Design, synthesis and biological evaluation of pyrimidine derivatives as novel CDK2 inhibitors that induce apoptosis and cell cycle arrest in breast cancer cells. Bioorg Med Chem. 2018;26(12):3491–3501.

18. Tantawy MA, Shalby AB, Barnawi IO, Kattan SW, Abd-Rabou AA, Elmegeed GA. Anti-cancer activity, and molecular docking of novel hybrid heterocyclic steroids revealed promising anti-hepatocellular carcinoma agent: implication of cyclin dependent kinase-2 pathway. Steroids. 2023;193:109187.
19. Nasr T, Bondock S, Youns M. Anticancer activity of new coumarin substituted hydrazide–hydrazone derivatives. Eur J Med Chem. 2014;76:539–548.
20. Ahmad Bhat A, Kaur G, Tandon N, Tandon R, Singh I. Current advancements in synthesis, anticancer activity, and structure–activity relationship (SAR) of coumarin derivatives. Inorg Chem Commun. 2024;167:112605.
21. Hassan RA, Hamed MIA, Abdou AM, El-Dash Y. Novel antiproliferative agents bearing substituted thieno[2,3-d] pyrimidine scaffold as dual VEGFR-2 and BRAF kinases inhibitors and apoptosis inducers; design, synthesis and molecular docking. Bioorg Chem. 2022;125:105861.
22. Mghwary AE-S, Hassan RA, Halim PA, Abdelhameid MK. Advances in structural identification of some thieno[2,3-d]pyrimidine scaffolds as antitumor molecules: synthetic approaches and control programmed cancer cell death potential. Bioorg Chem. 2025;154:107985.
23. Ismail MMF, El-Zahabi HSA, Ibrahim RS, Mehany ABM. Design and synthesis of novel tranilast analogs: docking, antiproliferative evaluation and in-silico screening of TGFβR1 inhibitors. Bioorg Chem. 2020;105:104368.
24. Mohamed MF, Saddiq AA, Al-Shaikh TM, Ibrahim NS, Abdelhamid IA. Computational studies and sever apoptotic bioactivity of new heterocyclic cyanoacrylamide based P-fluorophenyl and p-phenolic compounds against liver carcinoma (Hepg2). Bioorg Chem. 2021;114:105147.
25. Anwer KE, Sayed GH, Kozakiewicz-Piekarz A, Ramadan RM. Novel annulated thiophene derivatives: synthesis, spectroscopic, X-ray, Hirshfeld surface analysis, DFT, biological, cytotoxic and molecular docking studies. J Mol Struct. 2023;1276:134798.
26. Mosmann T. Rapid colorimetric assay for cellular growth and survival: application to proliferation and cytotoxicity assays. J Immunol Methods. 1983;65(1–2):55–63.
27. Hassan GS, Georgey HH, Mohammed EZ, George RF, Mahmoud WR, Omar FA. Mechanistic selectivity investigation and 2D-QSAR study of some new antiproliferative pyrazoles and pyrazolopyridines as potential CDK2 inhibitors. Eur J Med Chem. 2021;218:113389.
28. Sroor FM, Othman AM, Tantawy MA, Mahrous KF, El-Naggar ME. Synthesis, antimicrobial, anti-cancer and in silico studies of new urea derivatives. Bioorg Chem. 2021;112:104953.
29. Vermes I, Haanen C, Steffens-Nakken H, Reutelingsperger C. A novel assay for apoptosis flow cytometric detection of phosphatidylserine expression on early apoptotic cells using fluorescein labelled annexin V. J Immunol Methods. 1995;184(1):39–51.
30. Kim KH, Sederstrom JM. Assaying cell cycle status using flow cytometry. Curr Protoc Mol Biol. 2015;111(1):28.6.1–28.6.11.
31. Husseiny EM, S, Abulkhair, H, El-Dydamony, NM, Anwer KE. Exploring the cytotoxic effect and CDK-9 inhibition potential of novel sulfaguanidine-based azopyrazolidine-3,5-diones and 3,5-diaminoazopyrazoles. Bioorg Chem. 2023;133:106397.
32. Husseiny EM, Abulkhair HS, El-Sebaey SA, Sayed MM, Anwer KE. In vivo evaluation of novel synthetic pyrazolones as CDK9 inhibitors with enhanced pharmacokinetic properties. Future Med Chem. 2024;16(23):2487–2505.
33. Husseiny EM, Abdelnaby RM, Altwaijry N, Saleh A, Anwer KE. Comparison between conventional, grinding, and microwave synthesis of methylpyrazoles as VEGFR-2/HSP90 dual inhibitors. Future Med Chem. 2025;17(8):899–913.
34. Escabrós J, Crehuet R, Messeguer A. Studies on the toxic oil syndrome: proposal of a mechanism for the thermal conversion of 3-N-phenylamino-1,2-propanediol esters into anilides under deodorisation conditions. Tetrahedron. 2009;65(1):418–426.
35. Nabil Shabaan S, Saleh Alshehri F, Fadel Al-Rasheed J, El-Sebaey SA, Husseiny EM. Synthesis and exploration of new imidazo[4,5-c]pyrazoles as potent α-amylase inhibitors. ChemistrySelect. 2023;8(14):102313.
36. Ibrahim R, Ismail M, Shawer T, Ammar Y. Discovery of new quinoxalines as cytotoxic agents: design, synthesis and molecular modeling. Azhar Int J Pharm Med Sci. 2023;3(2):119–132.
37. Nawareg NA, Yassen ASA, Husseiny EM, El-Sayed MAA, Elshihawy HA. Exploring 1,2,3-triazole-Schiff's base hybrids as innovative EGFR inhibitors for the treatment of breast cancer: in vitro and in silico study. Bioorg Chem. 2025;155:108106.
38. Zheng J, Guo C, Ding H, Wu Y, Zhang K. A versatile method for preparing cyclic polyurethanes. React Funct Polym. 2025;206:106106.
39. Al-Wahaibi LH, Elbastawesy MAI, Abodya NE, Youssif BGM, Bräse S, Shabaan SN, Sayed GH, Anwer KE. New pyrazole/pyrimidine-based scaffolds as inhibitors of heat shock protein 90 endowed with apoptotic anti-breast cancer activity. Pharmaceuticals. 2024;17(10):1284.
40. Anwer KE, Sayed GH. Design, synthesis, antimicrobial, anticancer, and molecular docking of novel quinoline derivatives. Russ J Org Chem. 2024;60(5):956–969.
41. Alsulaimany M, Aljohani AKB, Abd El-Sattar NEA, Almadani SA, Alatawi OM, Alharbi HY, Aljohani MS, Al-Shareef AH, Alghamdi R, Tayeb SM, et al. Dual VEGFR-2 and EGFR T790M inhibitors of phenyldiazenes: anticancer evaluations, ADMET, docking, design and synthesis. Future Med Chem. 2025;17(3):287–300.

42. Naguib HM, Dauoud NT, Shaban SN, Abdelghaffar NF, Sayed GH, Anwer KE. Synthesis of pyrazolone derivatives by grinding, microwave, and conventional techniques and their antimicrobial activity. Russ J Org Chem. 2022;58(6):891–904.
43. Anwer KE, Hamza ZK, Ramadan RM. Synthesis, spectroscopic, DFT calculations, biological activity, SAR, and molecular docking studies of novel bioactive pyridine derivatives. Sci Rep. 2023;13(1):15598.
44. Anwer KE, Sayed GH, Essa BM, Selim AA. Green synthesis of highly functionalized heterocyclic bearing pyrazole moiety for cancer-targeted chemo/radioisotope therapy. BMC Chem. 2023;17(1):139.
45. Anwer KE, Sayed GH, Ramadan RM. Synthesis, spectroscopic, DFT calculations, biological activities and molecular docking studies of new isoxazolone, pyrazolone, triazine, triazole and amide derivatives. J Mol Struct. 2022;1256:132513.
46. Anwer KE, El-Sattar NEAA, Shamaa MM, Zakaria MY, Beshay BY. Design, green synthesis and tailoring of vitamin E TPGS augmented niosomal nano-carrier of pyrazolopyrimidines as potential anti-liver and breast cancer agents with accentuated oral bioavailability. Pharmaceuticals. 2022;15(3):330.
47. Abbas SE, Abdel Gawad NM, George RF, Akar YA. Synthesis, antitumor and antibacterial activities of some novel tetrahydrobenzo[4,5]thieno[2,3-d]pyrimidine derivatives. Eur J Med Chem. 2013;65:195–204.
48. Gediya P, Vyas VK, Carafa V, Sitwala N, Della Torre L, Poziello A, Kurohara T, Suzuki T, Sanna V, Raguraman V, et al. Discovery of novel tetrahydrobenzo[b]thiophene-3-carbonitriles as histone deacetylase inhibitors. Bioorg Chem. 2021;110:104801.
49. Arora S, Upadhayay S, Kumar P, Kumar P, Kumar R. Design, synthesis and anticancer evaluation of 4-substituted 5,6,7,8-tetrahydrobenzo[4,5]thieno[2,3-d]pyrimidines as dual topoisomerase I and II inhibitors. Bioorg Chem. 2025;154:108043.
50. Tadesse S, Anshabo AT, Portman N, Lim E, Tilley W, Caldon CE, Wang S. Targeting CDK2 in cancer: challenges and opportunities for therapy. Drug Discov Today. 2020;25(2):406–413.
51. Sviderskiy VO, Blumenberg L, Gorodetsky E, Karakousi TR, Hirsh N, Alvarez SW, Terzi EM, Kaparos E, Whiten GC, Ssebyala S, et al. Hyperactive CDK2 activity in basal-like breast cancer imposes a genome integrity liability that can be exploited by targeting DNA polymerase ε. Mol Cell. 2020;80(4):682–698.e7.
52. Indrayanto G, Putra GS, Suhud F. Validation of in-vitro bioassay methods: application in herbal drug research. Profiles Drug Subst Excip Relat Methodol. 2021;46:273–307.
53. Ismail MMF, Husseiny EM, Ibrahim MH. Mimicry of sorafenib: novel diarylureas as VEGFR2 inhibitors and apoptosis inducers in breast cancer. New J Chem. 2023;47(24):11565–11576.
54. Abdulrahman FG, Abulkhair HS, Zidan RA, Alwakeel AI, Al-Karmalawy AA, Husseiny EM. Novel benzochromenes: design, synthesis, cytotoxicity, molecular docking and mechanistic investigations. Future Med Chem. 2024;16(2):105–123.
55. Abdulrahman FG, Abulkhair HS, Saeed HSE, El-Dydamony NM, Husseiny EM. Design, synthesis, and mechanistic insight of novel imidazolones as potential EGFR inhibitors and apoptosis inducers. Bioorg Chem. 2024;144:107105.
56. Husseiny EM, Abulkhair HS, Saleh A, Altwaijry N, Zidan RA, Abdulrahman FG. Molecular overlay-guided design of new CDK2 inhibitor thiazepinopurines: synthesis, anticancer, and mechanistic investigations. Bioorg Chem. 2023;140:106789.
57. Patel DA, Patel SS, Patel HD. Advances in synthesis and biological evaluation of CDK2 inhibitors for cancer therapy. Bioorg Chem. 2024;143:107045.
58. Alamshany ZM, Tashkandi NY, Othman IMM, Anwar MM, Nossier ES. Bioorganic chemistry new thiophene, thienopyridine and thiazoline-based derivatives: design, synthesis and biological evaluation as antiproliferative agents and multitargeting kinase inhibitors. Bioorg Chem. 2022;127:105964.
59. El-Meguid EAA, El-Deen EMM, Moustafa GO, Awad HM, Nossier ES. Bioorganic chemistry synthesis, anticancer evaluation and molecular docking of new benzothiazole scaffolds targeting FGFR-1. Bioorg Chem. 2022;119;105504.
60. Kassem AF, Omar MA, Nossier ES, Awad HM, El-Sayed WA. Novel pyridine–thiazolidinone–triazole hybrid glycosides targeting EGFR and CDK-2: design, synthesis, anticancer evaluation, and molecular docking simulation. J Mol Struct. 2023;1294(P2):136358.
61. El-Sayed WA, Alminderej FM, Mounier MM, Nossier ES, Saleh SM, Kassem AF. New 1,2,3-triazole-coum arin-glycoside hybrids and their 1,2,4-triazolyl thioglycoside analogs targeting mitochondria apoptotic pathway: synthesis, anticancer activity and docking simulation. Molecules. 2022;27(17):1–29.
62. El-Sayed AA, Nossier ES, Almehizia AA, Amr AEE. Design, synthesis, anticancer evaluation and molecular docking study of novel 2,4-dichlorophenoxymethyl-based derivatives linked to nitrogenous heterocyclic ring systems as potential CDK-2 inhibitors. J Mol Struct. 2022;1247:131285.